ADVANCES IN ATMOSPHERIC SCIENCES, VOL. 34, JUNE 2017, 737–756

• **Original Paper** •

Nonlinearity Modulating Intensities and Spatial Structures of Central Pacific and Eastern Pacific El Niño Events

Wansuo DUAN[1], Chaoming HUANG[1,2], and Hui XU[*1]

[1] *State Key Laboratory of Numerical Modeling for Atmospheric Sciences and Geophysical Fluid Dynamics (LASG), Institute of Atmospheric Physics, Chinese Academy of Sciences, Beijing* 100029*, China*

[2] *University of Chinese Academy of Sciences, Beijing* 100049*, China*

(Received 14 June 2016; revised 30 January 2017; accepted 13 February 2017)

ABSTRACT

This paper compares data from linearized and nonlinear Zebiak–Cane model, as constrained by observed sea surface temperature anomaly (SSTA), in simulating central Pacific (CP) and eastern Pacific (EP) El Niño. The difference between the temperature advections (determined by subtracting those of the linearized model from those of the nonlinear model), referred to here as the nonlinearly induced temperature advection change (NTA), is analyzed. The results demonstrate that the NTA records warming in the central equatorial Pacific during CP El Niño and makes fewer contributions to the structural distinctions of the CP El Niño, whereas it records warming in the eastern equatorial Pacific during EP El Niño, and thus significantly promotes EP El Niño during El Niño–type selection. The NTA for CP and EP El Niño varies in its amplitude, and is smaller in CP El Niño than it is in EP El Niño. These results demonstrate that CP El Niño are weakly modulated by small intensities of NTA, and may be controlled by weak nonlinearity; whereas, EP El Niño are significantly enhanced by large amplitudes of NTA, and are therefore likely to be modulated by relatively strong nonlinearity. These data could explain why CP El Niño are weaker than EP El Niño. Because the NTA for CP and EP El Niño differs in spatial structures and intensities, as well as their roles within different El Niño modes, the diversity of El Niño may be closely related to changes in the nonlinear characteristics of the tropical Pacific.

Key words: El Niño diversity, nonlinearity, intensity, spatial structures, nonlinear temperature advection

Citation: Duan, W. S., C. M. Huang, and H. Xu, 2017: Nonlinearity modulating intensities and spatial structures of central Pacific and eastern Pacific El Niño events. *Adv. Atmos. Sci.*, **34**(6), 737–756, doi: 10.1007/s00376-017-6148-9.

1. Introduction

El Niño–Southern Oscillation (ENSO) is the most prominent ocean–atmosphere coupled system in the tropical Pacific. It exerts a strong impact on global weather and climate and often serves as a precursor to extreme weather and climate (Rasmusson and Wallace, 1983; Larkin and Harrison, 2005; McPhaden et al., 2006; Kim et al., 2009; Yeh et al., 2009). It is therefore extremely important to understand ENSO more comprehensively. Several theories have been proposed to explain ENSO (Bjerknes, 1969; Battisti, 1988; Jin, 1997a, 1997b; Weisberg and Wang, 1997; Wang, 2001; Wang and Picaut, 2004), and many mathematical models have been developed to simulate and predict it (Zebiak and Cane, 1987; Rosati et al., 1997; Latif et al., 1998; Yeh et al., 2012; Lopez and Kirtman, 2014). Although significant progress in this field has been achieved, considerable uncertainties in ENSO forecasting still remain. For example, in 2014, many ENSO forecast systems predicted a moderate El Niño year when only neutral conditions were experienced, and the extremely strong 2015/16 El Niño event was originally forecasted to be a weak or, at most, slightly strong El Niño event. Furthermore, after the 1990s, the frequent occurrence of a new type of El Niño event further increased the uncertainties involved in forecasting ENSO. This new type of El Niño is often referred to as "CP El Niño" (CP: central Pacific), since its maximum sea surface temperature anomaly (SSTA) is located in the central equatorial Pacific (Kao and Yu, 2009). It has also been variously termed "dateline El Niño" (Larkin and Harrison, 2005), "El Niño Modoki" (Ashok et al., 2007; Takahashi et al., 2011) or "warm pool El Niño" (Kug et al., 2009). CP El Niño events are different from conventional El Niño events, which are referred to as "EP El Niño" (EP: eastern Pacific) (Rasmusson and Carpenter, 1982) owing to their feature of a warm SSTA centered in the eastern Pacific. CP El Niño events significantly influence weather and climate throughout many parts of the globe, but in a manner different than that of EP El Niño events (Weng et al., 2007; Kim et al., 2009; Lee and McPhaden, 2010; Mo,

* Corresponding author: Hui XU
Email: xuh@lasg.iap.ac.cn

2010; Yu et al., 2010; Feng and Li, 2011; Wang and Wang, 2013). Many studies have attempted to better understand the physics of El Niño events, but most can only explain those of EP El Niño events [see the review of Wang and Picaut (2004)]. Because CP El Niño events significantly influence weather and climate in a different manner than EP El Niño events, it is necessary to better constrain the physics of CP El Niño events and to more fully identify differences between CP and EP El Niño events.

Many studies have attempted to better understand CP El Niño events (Ashok et al., 2007; Kao and Yu, 2009; Kug et al., 2009; Yeh et al., 2009, Lee and McPhaden, 2010). Xiang et al. (2013) and Chung and Li (2013) argued that the frequent occurrence of CP El Niño events can be attributed to the recent La Niña-like climatological mean state [also see Duan et al. (2014)]. Other researchers have suggested that extratropical forcing plays an important role in the generation of CP El Niño (Yu et al., 2010; Kim et al., 2012). Some studies have emphasized that the increasing frequency of CP El Niño events during the past decade is related to global warming caused by anthropogenic forcing (Yeh et al., 2009; Na et al., 2011). To explain the formation of the CP El Niño mode, Kug et al. (2009) suggested that zonal temperature advection feedback plays a crucial role in the development and decay of the SSTA, since thermocline feedback is known to represent a key process of EP El Niño. However, Chen et al. (2015) demonstrated that the diversity of El Niño events results from the random occurrence of westerly wind bursts. Therefore, the physics of CP El Niño events still remains controversial.

When compared with EP El Niño events, CP El Niño events are often much weaker and feature patterns with warm centers located much more centrally in the equatorial Pacific. Previous studies have illustrated that nonlinear temperature advection processes exert a significant impact on the intensities of EP El Niño events. This nonlinear temperature advection enhances the intensities of EP El Niño events while suppressing those of La Niña events, eventually resulting in El Niño and La Niña events producing asymmetrical amplitudes (An and Jin, 2004; Duan et al., 2004, 2008; Duan and Mu, 2006; Su et al., 2010). The nonlinear temperature advection occurring in the ENSO model is a nonlinear term, and its effects dominate the nonlinearity of ENSO (Duan et al., 2008). The goal of this paper is to therefore address a series of questions related to this term: Does the nonlinear temperature advection also modulate the intensities of CP El Niño events? Can it explain why CP El Niño events are often weaker than EP El Niño events? And does the nonlinear temperature advection exert any influence on the spatial pattern of CP El Niño events?

To investigate the role of nonlinearity in modulating the intensities of El Niño events, many studies (e.g., An and Jin, 2004) have used observational data to directly compute the nonlinear terms of control equations of state variables and then to determine the role of nonlinearity. However, this approach cannot comprehensively evaluate the entire role of nonlinear temperature advection. Therefore, to better constrain this nonlinearity, we derive a series of equations (Appendix A). These functions demonstrate that nonlinearity can induce changes in state variables. However, these state variables exist not only within nonlinear terms but also within the linear terms of state equations. Therefore, changes in state variables caused by nonlinearity can also be reflected in linear terms. In other words, nonlinear effects are reflected not only in the nonlinear terms of state equations but also in state-dependent linear terms. Thus, by only evaluating nonlinear terms to investigate the effects of nonlinearity, it is possible to neglect nonlinear effects attributable to state-dependent linear terms. However, by linearizing a nonlinear model and then comparing the nonlinear model and its linearized version, it is possible to determine the full role of nonlinearity and to add new insights to the results of previous studies. Therefore, in the present study, we adopt this new approach to investigate the role of nonlinearity more fully.

Many coupled climate models simulate CP El Niño events with some biases (Yeh et al., 2009; Kug et al., 2012; Bellenger et al., 2014; Taschetto et al., 2014), and therefore do not represent platforms for studying the CP El Niño phenomenon, relative to that of EP El Niño. Recently, Duan et al. (2014) proposed an approach using an optimal forcing vector (OFV; see Appendix B) to forcefully reproduce observed CP El Niño events. Specifically, Duan et al. (2014) computed an external forcing term superimposed on the tendency equation of the Zebiak–Cane model (Zebiak and Cane, 1987). This method corrects the model simulations closest to observed data, thus using observational data to reproduce observed CP El Niño events. Based on these reproduced CP El Niño events, Duan et al. (2014) explored the physics of CP El Niño and demonstrated that the La Niña-like climatological mean state is one of the climatological conditions responsible for the frequent occurrence of CP El Niño events. Tian and Duan (2016) then determined the optimal observation locations that improve upon the current "spring predictability barrier" used to forecast the two types of El Niño events. Clearly, reproducing CP El Niño events using the OFV approach represents a foundation for future studies of CP El Niño physics and predictability. In this paper, we follow the approach of Duan et al. (2014) to reproduce CP El Niño events and to explore how the nonlinearity associated with nonlinear temperature advection modulates the intensities and spatial structures of CP El Niño. In section 2, we use the Zebiak–Cane model to reproduce observed CP and EP El Niño events using the OFV approach. The roles of nonlinearity in modulating the intensities and spatial structures of these reproduced CP and EP El Niño events are then explored in section 3. Section 4 compares CP and EP El Niño events to identify the different impacts of nonlinearity in modulating their intensities and spatial structures. Finally, a summary and discussion of these data are presented in section 5.

2. Reproducing observed CP and EP El Niño events with the Zebiak–Cane model

The Zebiak–Cane model is a nonlinear anomaly model with intermediate complexity that describes atmospheric and

oceanic anomalies about a monthly mean climatological state. Since successfully predicting the 1986–87 El Niño events, this model has been widely used to study ENSO dynamics and predictability, thus serving as a benchmark in ENSO research for decades (Zebiak and Cane, 1987; Chen et al., 2004; Tang et al., 2008; Duan et al., 2014). However, most resulting studies have focused on EP El Niño events (Chen et al., 1995, 2004), with even fewer studies using the Zebiak–Cane model to simulate CP El Niño events, likely due to the effects of model errors. Li et al. (2013) argued that the tropical Pacific cold-tongue cooling mode might be an important factor in the triggering of frequent CP El Niño occurrences in recent decades. Some studies have also demonstrated that wind forcing from the subtropical and extratropical atmosphere may play an important role in the occurrence of CP El Niño events (e.g., Yu et al., 2010; Kug et al., 2012). Regardless, all these factors associated with CP El Niño events are absent from the Zebiak–Cane model, consequently causing additional model errors.

The climatological mean state of the Zebiak–Cane model includes the components of monthly mean SST, surface currents, upwelling, thermocline depth, and annual mean vertical temperature gradient and thermocline depth. Monthly mean SST is specified using observations from the Climate Analysis Center dataset made from 1950 to 1979 (Rasmusson and Carpenter, 1982); monthly mean surface currents are generated by spinning the ocean component model with monthly mean climatological wind data assembled by Rasmusson and Carpenter (1982); and monthly mean upwelling is calculated using mean surface currents according to a simple functional relationship. The annual mean thermocline depth and vertical temperature gradient are calculated by the vertical temperature profile estimated from observations [more details can be found in Zebiak and Cane (1987)]. Duan et al. (2014) indicated that the Zebiak–Cane model cannot reproduce CP El Niño events very well, even when using observations made during the past 30 years (during which time CP El Niño events have frequently occurred) to generate these climatological annual cycles. This indicates that model errors limiting the simulation of CP El Niño originate from multiple sources, and not only from the climatological annual cycle bias. Furthermore, these sources are likely mixed and cannot be easily separated. In this study, we still use the climatological annual cycle generated using data gathered from 1950 to 1979, and follow the technique of Duan et al. (2014) to consider the combined effects of different model errors. The technique involves adding an external OFV to the SSTA governing equation, in an attempt to reduce the model bias of the climatological mean state, and correcting for the absence of relevant physical processes by assimilating a series of HadISST (Hadley Center Global Sea Ice and Sea Surface Temperature) analytical data (Rayner et al., 2003). The construction of this model thus ultimately yields a simulation of CP El Niño events. In this approach, use of an appropriate initial value can avoid in a resulting OFV that is too large, thus not permitting us to obtain the relevant state variables needed to satisfy dynamics and/or physics. The initialization procedure developed by Chen et al. (1995) used within the Zebiak–Cane model has proven to be highly effective in hindcasting El Niño events (Chen et al., 2004). Therefore, in this paper, we adopt this initialization procedure to obtain the initial conditions of the Zebiak–Cane model starting on 1 January of an El Niño year (i.e., the year during which the El Niño event peaks) and to compute the OFV associated with each CP El Niño event. This OFV is then superimposed on the tendency of the model temperature equation to correct the model for reproducing CP El Niño events occurring from 1980 to 2010, including the 1990/91, 1994/95, 2002/03, 2004/05, and 2009/10 CP El Niño events (Fig. 1). As a comparison, we also use a similar approach to reproduce three observed EP El Niño events during this period (namely, the 1982/83, 1986/87, 1997/98 EP El Niño events), and plot their corresponding SSTA values in Fig. 2. Because the 1972/73 El Niño is a typically strong EP El Niño event, we also examine this event in the present study.

Figures 1 and 2 demonstrate that reproduced El Niño events generated by the Zebiak–Cane model with the corresponding OFV present SSTA values well correlated with observed data, whereas those generated without OFVs do not fit these observations well, and some even fail to become El Niño events. For example, the 1982/83, 1986/87, and 1997/98 EP El Niño cases generated by the Zebiak–Cane model without OFVs appear to fit observations reasonably well, whereas the 1972/73 EP El Niño event predicted by the Zebiak–Cane model without an OFV exhibits only a very weak warming signal in the equatorial central Pacific and ultimately fails to become an El Niño event. However, any CP El Niño case reproduced by the Zebiak–Cane model without an OFV is not acceptable.

Figure 3 compares the magnitude of the OFVs to the terms in the temperature equation of the Zebiak–Cane model for five CP El Niño events. Because the warming signal of CP El Niño events mostly occurs in the Niño4 region (5°N–5°S, 160°E–150°W), the related OFVs and equation terms are calculated by averaging over this region. These results demonstrate that the values of the OFVs usually yield comparable amplitudes to those of the terms of the Zebiak–Cane model, and therefore may play an important role in modulating CP El Niño events (Fig. 3b). Furthermore, the Zebiak–Cane model with OFVs tends to reproduce CP El Niño events, whereas without OFVs it fails to generate them (Fig. 1). Additionally, OFVs associated with CP El Niño events consistently exhibit an SSTA tendency pattern with positive anomalies in the equatorial eastern Pacific, thus indicating that SST tendency errors occurring in the equatorial eastern Pacific dominate the uncertainties of the Zebiak–Cane model when simulating CP El Niño events [more details can be found in Duan et al. (2014)]. In analyzing CP El Niño–related model uncertainties offset by OFVs, Duan et al. (2014) demonstrated that one of the model uncertainties offset by OFVs is the absence of a climatological SST cold-tongue cooling mode in the Zebiak–Cane model. When these researchers replaced the original climatological annual cycle with one including a climatological SST cold-tongue cooling mode, the Zebiak–

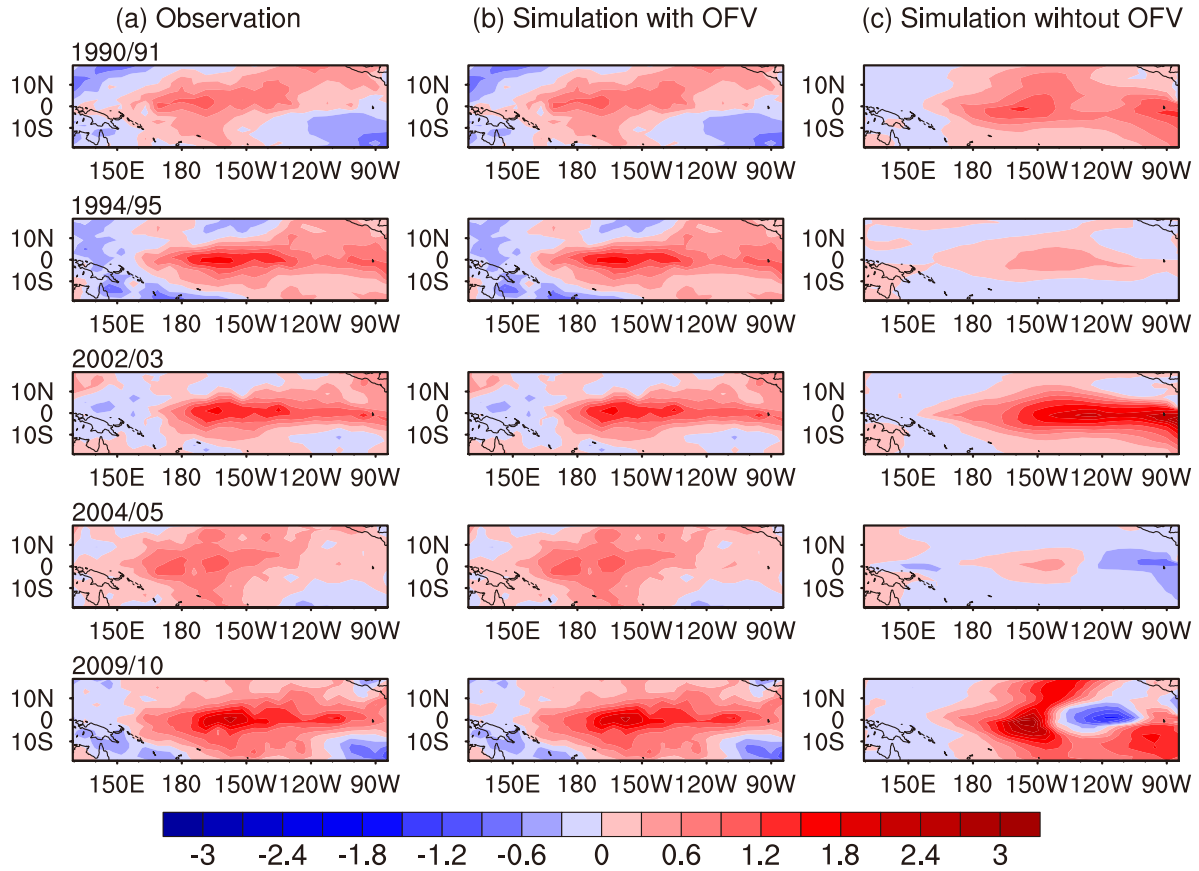

Fig. 1. SSTAs in the mature phase of five CP El Niño events (units: °C): (a) observed El Niño; (b) El Niño reproduced by the nonlinear Zebiak–Cane model with an OFV; (c) El Niño reproduced by the nonlinear Zebiak–Cane model without an OFV. The mature phases here are the months when the El Niño events peak, which are January 1991, January 1995, November 2002, January 2005, and January 2010.

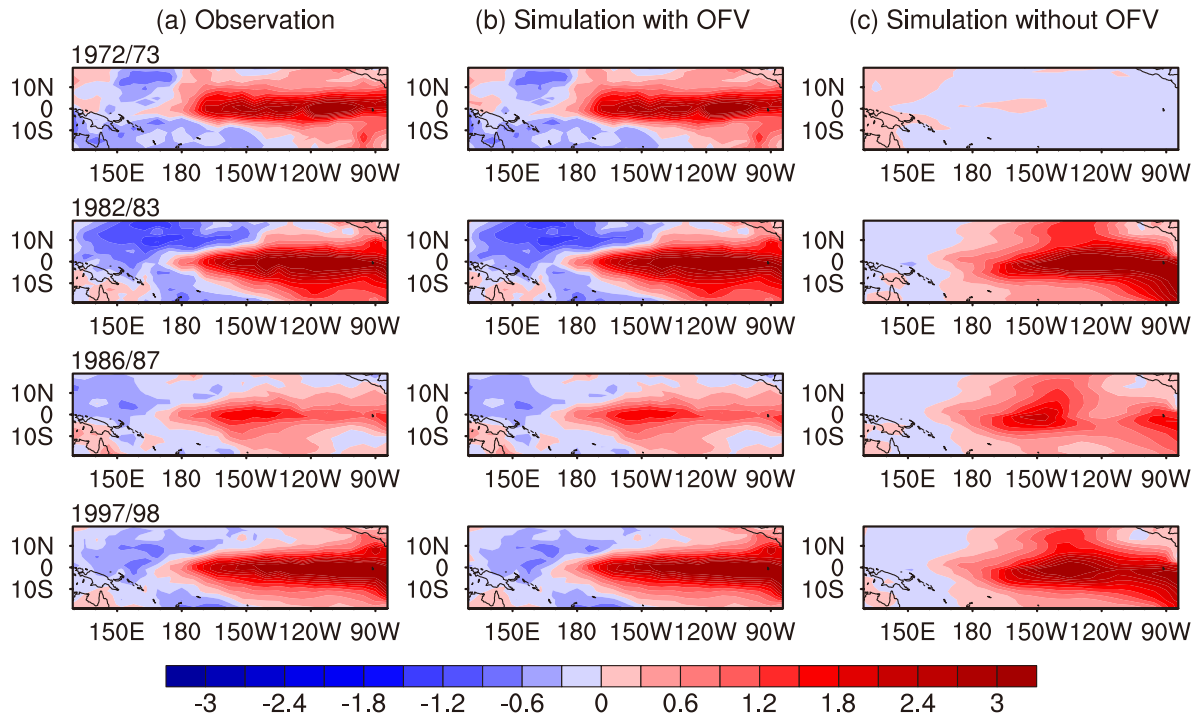

Fig. 2. SSTAs in the mature phase for four EP El Niño events (units: °C): (a) observed El Niño; (b) El Niño reproduced by the nonlinear Zebiak–Cane model with an OFV; (c) El Niño reproduced by the nonlinear Zebiak–Cane model without an OFV. The mature phases here are the months when the El Niño events peak, which are January 1972, 1983, 1987, and 1998.

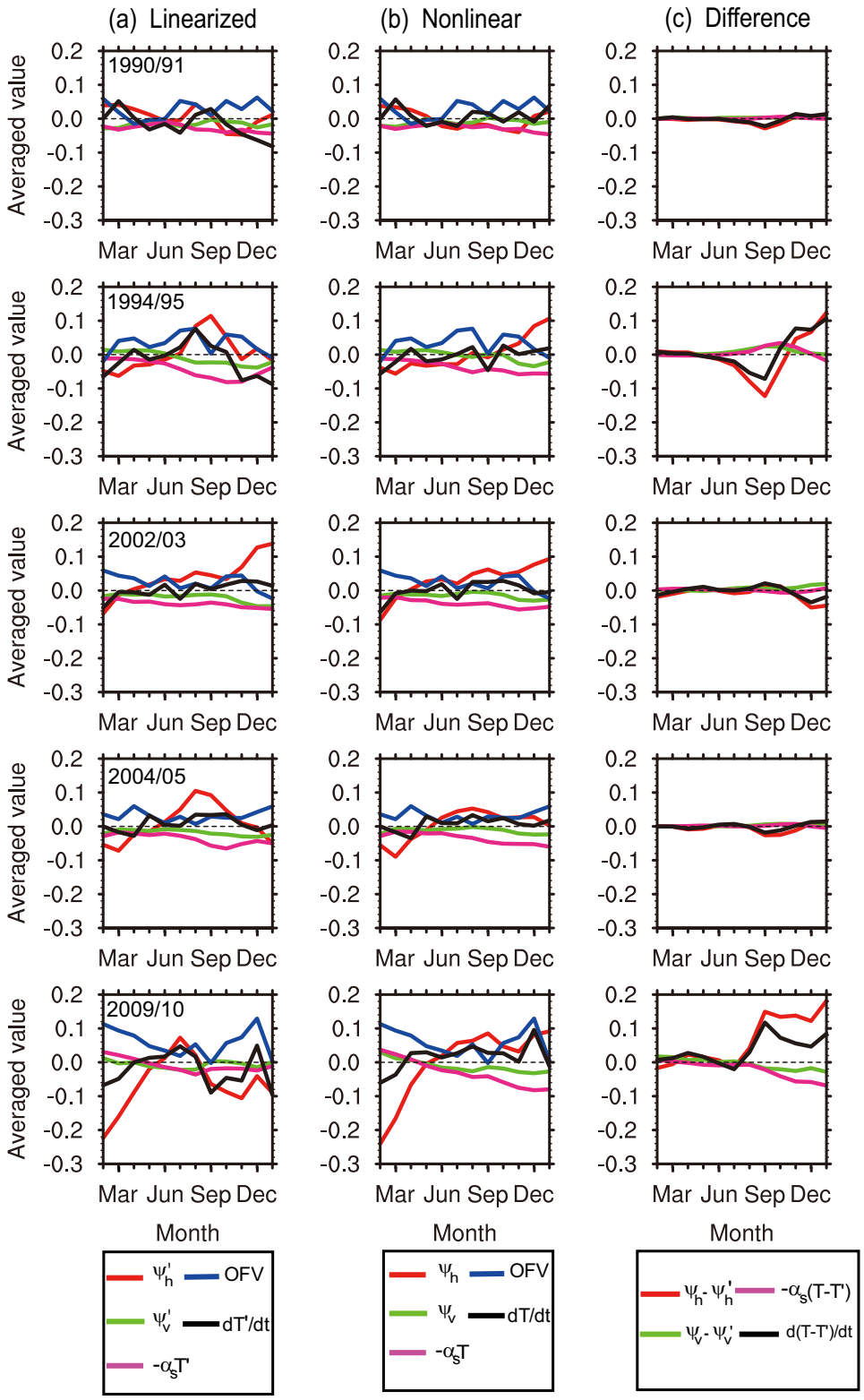

Fig. 3. (a) Time series of horizontal temperature advection (red line), vertical temperature advection (green line), damping term (pink line), and total SSTA tendency (black line), for CP El Niño-like events generated by the linearized Zebiak–Cane model, obtained by averaging over the Niño4 region (5°N–5°S, 160°E–150°W) [units: °C (10 d)$^{-1}$]. (b) As in (a) but for CP El Niño events reproduced by the nonlinear Zebiak–Cane model. The OFV (blue line) in (b) is the same as in (a). The lines in (c) are obtained by determining the differences between (b) and (a) and illustrate the horizontal (red line) and vertical (green line) NTA values, the nonlinearly induced damping term change (pink line), and the nonlinearly induced SSTA tendency change (black line).

Cane model produced SSTA patterns with warming centers departing from the east coast but still located far from the dateline. These results indicate that the model uncertainties offset by the OFV cannot be solely attributed to the SST cold-tongue mode, but are also affected by other sources of uncertainties. For example, as mentioned in section 2, the Zebiak–Cane model cannot fully describe the effects on CP El Niño of subtropical and extratropical atmospheric conditions, which have been shown to be important to CP El Niño events but are absent in the Zebiak–Cane model. This oversight introduces additional model uncertainties, which can also be offset by the OFV.

Figure 4b demonstrates that, for EP El Niño events, OFVs are often smaller than the terms in the Zebiak–Cane model. Particularly, with the development of El Niño events, amplitudes of OFVs become significantly smaller than those of temperature advection terms. Furthermore, these OFVs even yield negative values during the latter periods of strong El Niño years (1972/73, 1982/83 and 1997/98), and thus cannot be responsible for the intensification of intensities of El Niño events in a nonlinear regime (see section 3). Regardless, the role of OFVs in modulating these EP El Niño events is not negligible. For example, the Zebiak–Cane model run without corresponding OFVs fails to reproduce the 1972/73 El Niño event, but the Zebiak–Cane model run with a corresponding OFV is able to do so (Fig. 2). Furthermore, Duan et al. (2014) indicated that patterns of OFVs depend on different EP El Niño events and do not exhibit a unified pattern.

Comparing Figs. 3 and 4 clearly demonstrates that differences between linear and nonlinear simulations in both EP and CP El Niño events are very small during the first half of an El Niño event (see Figs. 3c and 4c), thus indicating that the effect of nonlinearity is smaller during the first half of El Niño than it is during the second half. Furthermore, the amplitude of these differences in EP El Niño events is more than twice that observed for CP El Niño events. This implies that EP El Niño events are more significantly influenced than CP El Niño events by nonlinearity. To address how nonlinearity modulates CP and EP El Niño events, the present study therefore focuses on constraining the influence of nonlinear temperature advection on CP and EP El Niño events. As described above, OFVs can help reproduce observed El Niño events and generate acceptable simulations of related physical variables (Duan et al., 2014). Therefore, it is reasonable to use the CP and EP El Niño events reproduced by the corrected Zebiak–Cane model with the corresponding OFV to analyze the role of nonlinear temperature advection in modulating El Niño events. For simiplicity, from here on, when we refer to the "Zebiak–Cane model", we mean the Zebiak–Cane model with a corresponding OFV.

3. Modulation of the intensities and spatial structures of CP and EP El Niño events by nonlinearity

As previously mentioned, nonlinearity in the Zebiak–Cane model mainly arises from nonlinear temperature advection in the temperature equation. The SST anomaly equation in the (corrected) Zebiak–Cane model can be expressed as

$$\begin{aligned}\frac{\partial T}{\partial t} = &-\bar{u}T_x - \bar{v}T_y - \gamma M(\bar{w})T_z - u\overline{T}_x - v\overline{T}_y - \\ &\gamma[M(\bar{w}+w) - M(\bar{w})]\overline{T}_z - uT_x - vT_y - \\ &\gamma[M(\bar{w}+w) - M(\bar{w})]T_z - \alpha_s T + f\,, \end{aligned} \tag{1}$$

where T, u, v and w denote respectively anomalies of mixed layer temperature (or SST), horizontal surface zonal velocity, meridional velocity, and upwelling at the mixed layer base. γ is a parameter that describes the strength of upwelling with the value 0.75, and α_s is a nondimensional parameter that represents the Newtonian cooling coefficient for SSTA. The function $M(x)$ is defined by $M(x) = \begin{cases} 0, & x \leqslant 0; \\ x, & x > 0. \end{cases}$ An overbar in Eq. (5) denotes the climatological mean and "f" represents the OFV superimposed on the SST anomaly equation. This "f" is calculated with one-month intervals and covers the region with a 5.625° latitude ×2° longitude grid, with latitude ranging from 129.375°W to 84.375°W and longitude ranging from 19°S to 19°N. The temperature advection in Eq. (5) is denoted as

$$\begin{aligned}\Psi = &-\bar{u}T_x - \bar{v}T_y - \gamma M(\bar{w})T_z - u\overline{T}_x - v\overline{T}_y - \\ &\gamma[M(\bar{w}+w) - M(\bar{w})]\overline{T}_z - uT_x - vT_y - \\ &\gamma[M(\bar{w}+w) - M(\bar{w})]T_z\,. \end{aligned} \tag{2}$$

In this equation, $\Psi_{\rm h} = -\bar{u}T_x - \bar{v}T_y - u\overline{T}_x - v\overline{T}_y - uT_x - vT_y$ and $\Psi_{\rm v} = -\gamma M(\bar{w})T_z - \gamma[M(\bar{w}+w) - M(\bar{w})]\overline{T}_z - \gamma[M(\bar{w}+w) - M(\bar{w})]T_z$ are the horizontal and vertical components, respectively, of the temperature advection Ψ. In these temperature advections, $\Psi_{\rm n} = -uT_x - vT_y - \gamma[M(\bar{w}+w) - M(\bar{w})]T_z$ represents the nonlinear temperature advection term. To determine the influence of nonlinear temperature advection on the intensities and spatial structures of CP and EP El Niño events, we linearize the SSTA equation in the Zebiak–Cane model as follows:

$$\begin{aligned}\frac{\partial T'}{\partial t} = &-\bar{u}T'_x - \bar{v}T'_y - \gamma M(\bar{w})T'_z - u'\overline{T}_x - v'\overline{T}_y \\ &-\gamma[M(\bar{w}+w') - M(\bar{w})]\overline{T}_z - \alpha_s T' + f\,, \end{aligned} \tag{3}$$

where "f" is the same as that in Eq. (1), the prime denotes the variables in the linearized model, and the temperature advection term becomes

$$\begin{aligned}\Psi' = &-\bar{u}T'_x - \bar{v}T'_y - \gamma M(\bar{w})T'_z - u'\overline{T}_x - v'\overline{T}_y - \\ &\gamma[M(\bar{w}+w') - M(\bar{w})]\overline{T}_z\,, \end{aligned} \tag{4}$$

where $\Psi'_{\rm h} = -\bar{u}T'_x - \bar{v}T'_y - u'\overline{T}_x - v'\overline{T}_y$ and $\Psi'_{\rm v} = -\gamma M(\bar{w})T'_z - \gamma[M(\bar{w}+w') - M(\bar{w})]\overline{T}_z$ are the horizontal and vertical components, respectively, of the temperature advection in the linearized model. The nonlinear effect generated by the nonlinear temperature advection term is thus reflected in the temperature advection change $\Psi - \Psi'$, as well as the damping term change $-\alpha_s(T - T')$ (also see Appendix A). That is, Eq. (5) holds:

$$\frac{d(T - T')}{dt} = (\Psi - \Psi') - \alpha_s(T - T')\,. \tag{5}$$

Fig. 4. As in Fig. 3 but for EP El Niño events.

From the Eq. (5), it is clear that the influences of nonlinear temperature advection on the SSTA associated with CP and EP El Niño events (i.e., the differences between T and T'), are driven by the nonlinearly induced temperature advection change (NTA; $\Psi - \Psi'$). That is, the NTA is equal to $\Psi - \Psi'$, where $\Psi_h - \Psi'_h$ describes the horizontal component of the NTA, and $\Psi_v - \Psi'_v$ represents the vertical component. In contrast with the "linearized Zebiak–Cane model", we hereafter refer to the prementioned Zebiak–Cane model in section 2 as the "nonlinear Zebiak–Cane model". In any case, both of them are forced by the same OFV.

3.1. *CP El Niño events*

For the five reproduced CP El Niño events in the nonlinear Zebiak–Cane model, the related SSTA values are constrained to be close to the observed SSTA values. Here, we use the initial anomalies of these reproduced CP El Niño events as the initial values of the linearized Zebiak–Cane model, and then integrate the linearized model. By doing so, five SSTA time series can be obtained; the correspond-

ing evolution of SSTA along the equator (within the region of 5°N–5°S) is plotted in Fig. 5. This figure demonstrates that the five SSTA time series present CP El Niño-like events. By comparing their intensities with those obtained in the nonlinear model, we can observe that the 1990/91, 2002/03 and 2004/05 CP El Niño-like events do not change significantly in the nonlinear Zebiak–Cane model, but that the 1994/95 and 2009/10 CP El Niño-like events are significantly enhanced. The nonlinear Zebiak–Cane model includes the effects of nonlinearity, whereas the linearized model does not. As analyzed above, the nonlinearities of the Zebiak–Cane model are mainly reflected by the NTA ($\Psi - \Psi'$). Although the damping term change $[-\alpha_s(T - T')]$ is also related to nonlinearity, it plays either a negligible or a negative role in enhancing CP El Niño. Specifically, Fig. 3c demonstrates that nonlinearities from either the damping term change or the horizontal or vertical NTA are often negligible for the 1990/91, 2002/03 and 2004/05 CP El Niño-like events, and only exert minimal effects on the intensities of these El Niño events. However, in the 1994/95 and 2009/10 CP El Niño events, the corresponding horizontal NTA values are positive, whereas the vertical NTA and the damping term change tend to be negative, especially during their mature phases (i.e., in January of the 1994 and 2009 El Niño years). Furthermore, the amplitude of the former term is significantly larger than that of the latter two terms. These data therefore suggest that the positive and significantly large horizontal NTA values aggressively enhance the 1994/95 and 2009/10 CP El Niño events. This implies that the NTA plays an important role in enhancing strong CP El Niño events.

The above results are derived from values of relevant variables averaged throughout the Niño4 region. Figure 6 displays the time-dependent evolution of the NTA along the equator (within 5°N–5°S), and thus further illustrates how the NTA modulates CP El Niño events. It is this NTA that introduces differences between El Niño events generated by the nonlinear Zebiak–Cane model and those presented by its linearized model (see Fig. 5c). Figure 6 demonstrates that the positive NTA of five CP El Niño events first appears in the eastern equatorial Pacific and then moves westwards; eventually, the warming rate of the NTA occurs in the central equatorial Pacific during its mature phase. Figure 6 also demonstrates that the NTA often yields small values in the tropical central Pacific during the mature phases of the 1990/91, 2002/03 and 2004/05 CP-El Niño events (i.e., in January of the 1990 and 2004 El Niño years, but in November of the 2002 El Niño year), whereas it yields largely positive values during the mature phases of the 1994/95 and 2009/10 events. Therefore, the NTA does not significantly affect the intensities of the 1990/91, 2002/03, and 2004/05 CP El Niño events, but does significantly enhance those of the 1994/95 and 2009/10 events. This explains why the 1990/91, 2002/03 and 2004/05 CP El Niño-like events in the linearized Zebiak–Cane model do not significantly change in the nonlinear Zebiak–Cane model, whereas the 1994/95 and 2009/10 CP El Niño-like events are significantly enhanced. These results illustrate that the ability of nonlinearity to enhance these values mainly occurs during the mature phase of strong CP El Niño events. Additionally, Fig. 6a demonstrates that, during the evolution of the NTA, a band of negative values occurs, propagating westwards and sometimes preceding the positive band. This indicates that relevant CP El Niño events are suppressed by negative NTA values during their development phase, but are then enhanced by positive NTA, especially during their mature phase, which further emphasizes the enhanced role of the NTA in the mature phases of strong CP El Niño events.

Figure 6 also records the time-dependent evolution of the horizontal and vertical components of the NTA along the equator (within 5°N–5°S). This figure demonstrates that the evolution of the horizontal NTA in the tropical Pacific is very similar to that of the total NTA, thus implying that the horizontal NTA component contributes the most to the total NTA value. Especially during the mature phases of the 1994/95 and 2009/10 CP El Niño events, the NTA in the tropical Pacific exhibits significantly large positive values, with the horizontal NTA component making the greatest contributions to it. Although the vertical NTA component is positive during the developing phase of the El Niño events, and therefore enhances the 1994/95 and 2009/10 CP El Niño events, there is a less notable difference in amplitude between the values of strong CP El Niño events (i.e., 1994/95 and 2009/10) and weak ones (i.e., 1990/91, 2002/03 and 2004/05). In contrast, the horizontal NTA values show considerable differences in their amplitudes, especially during the mature phases of these events (Figs. 3 and 6). These results may indicate that, during the mature phase of an event, the horizontal NTA plays a major role in enhancing the intensity of a CP El Niño event, whereas the vertical NTA exerts a secondary influence. Figure 7 displays the NTA, and its horizontal and vertical components, during the mature phases of five CP El Niño events. This figure illustrates that the warm center of the NTA is located in the tropical central Pacific, especially in the Niño4 region; this is the location of the warm center of CP El Niño events, and thus indicates that the positive NTA (and especially the positive horizontal NTA) in the tropical central Pacific is responsible for enhancing the intensity of CP El Niño events. Furthermore, the vertical NTA components of the 1994/95 and 2009/10 CP El Niño events exhibit obvious cooling rates in the eastern equatorial Pacific during their mature phases, thus decreasing the SSTAs in the eastern equatorial Pacific and serving as foils to the intensification of related SSTAs in the Niño4 region.

The positive NTA, and especially the positive horizontal NTA, observed in the Niño4 region during the mature phases of CP El Niño events, tends to produce additional positive SSTA values in the same area. These values, along with those of the negative anomalies of the vertical NTA in the eastern equatorial Pacific, increase the gradient of the SSTA between the equatorial central and the western Pacific, as well as that of the SSTA between the equatorial central and the eastern Pacific. This former condition is favorable for increasing anomalous westerly wind and favors warm water in the western Pacific moving eastwards, whereas the latter con-

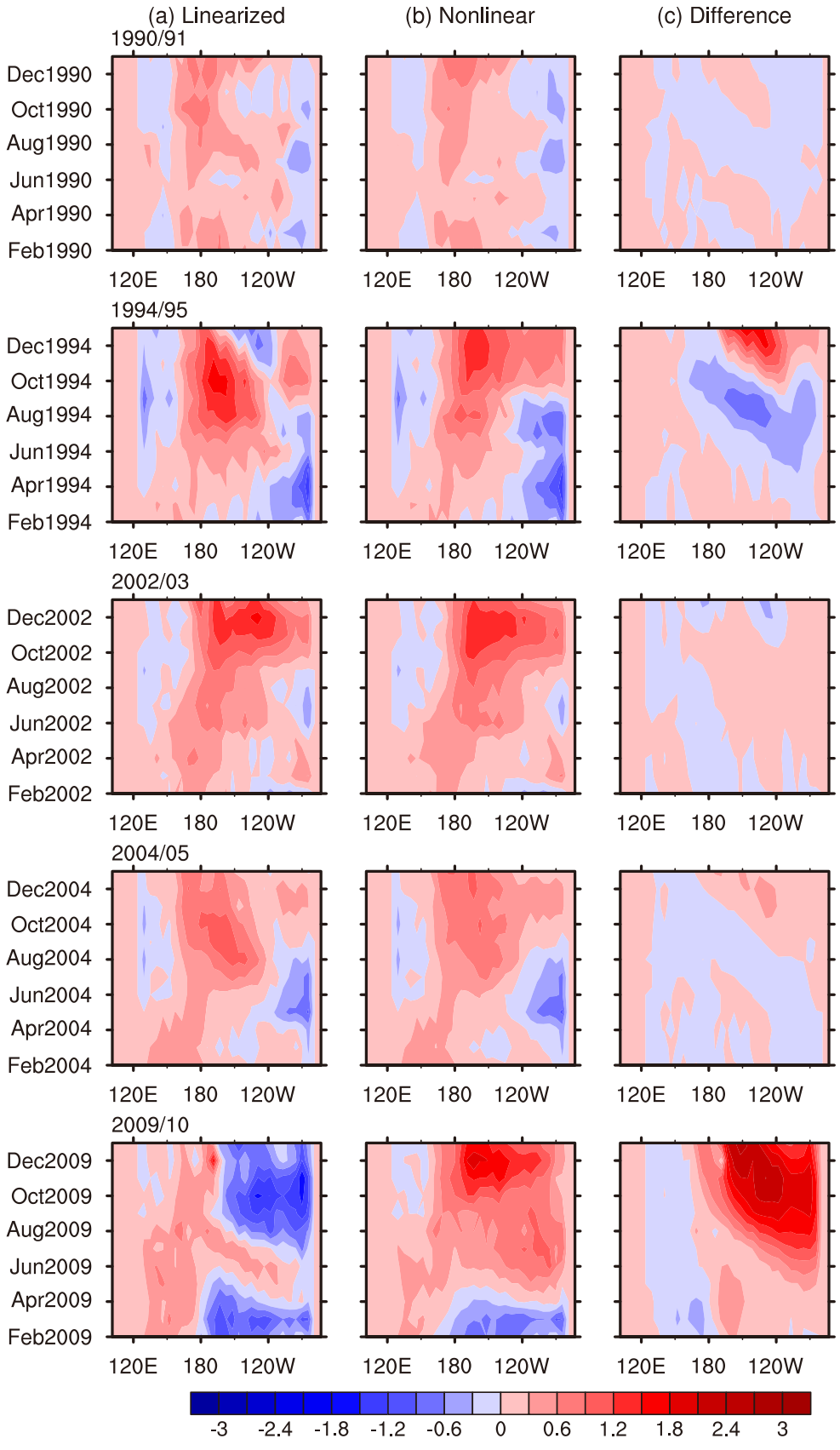

Fig. 5. Evolution of the SSTA [units: °C (10 d)$^{-1}$] along the equator (within 5°N–5°S) for five CP El Niño events: (a) results of El Niño events generated by the linearized Zebiak–Cane model; (b) results of El Niño events reproduced by the nonlinear Zebiak–Cane model; and (c) differences between (b) and (a).

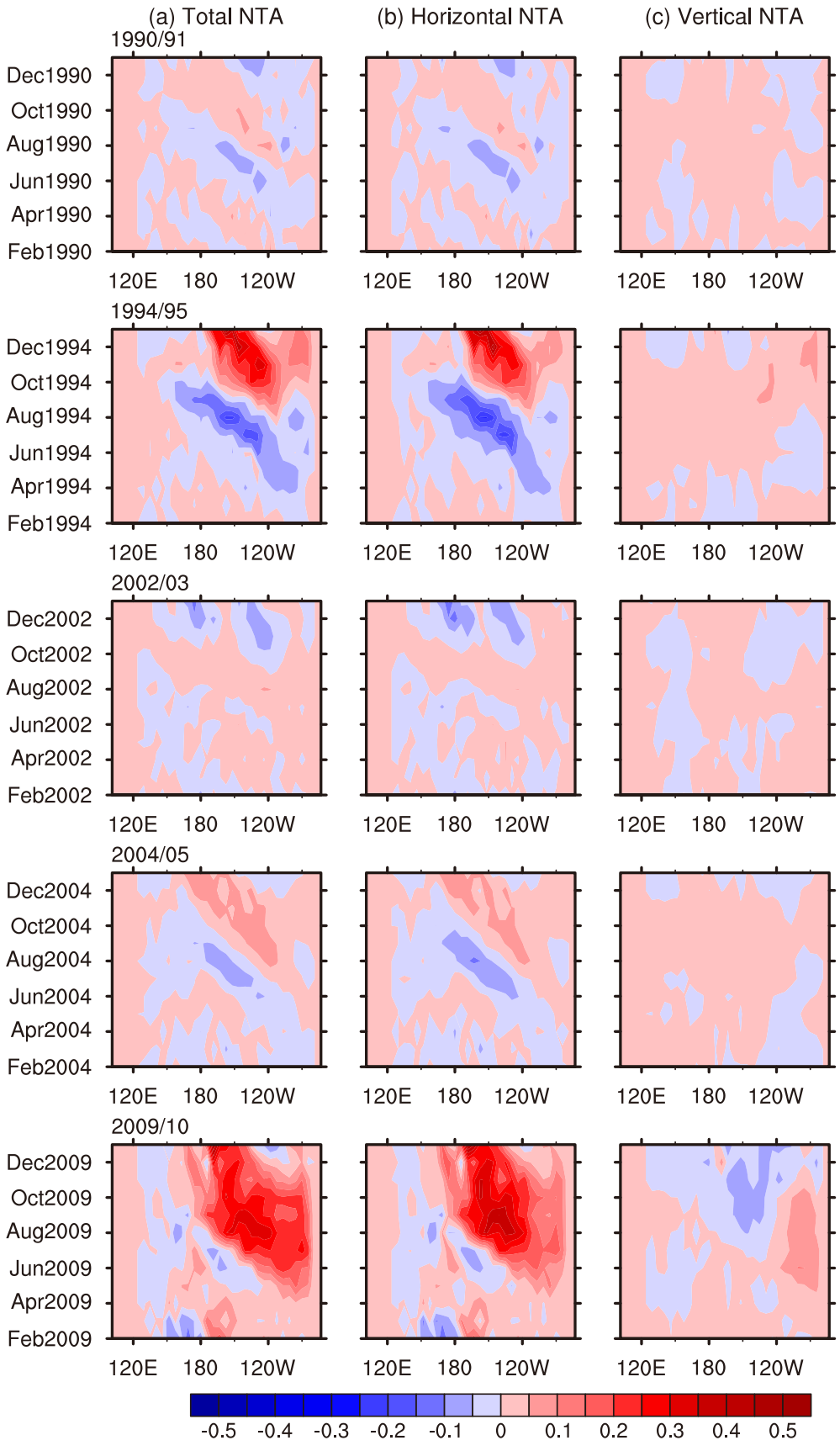

Fig. 6. Evolution of (a) the total NTA [units: °C (10 d)$^{-1}$] and (b) its horizontal and (c) vertical components along the equator (within 5°N–5°S) for five CP El Niño events.

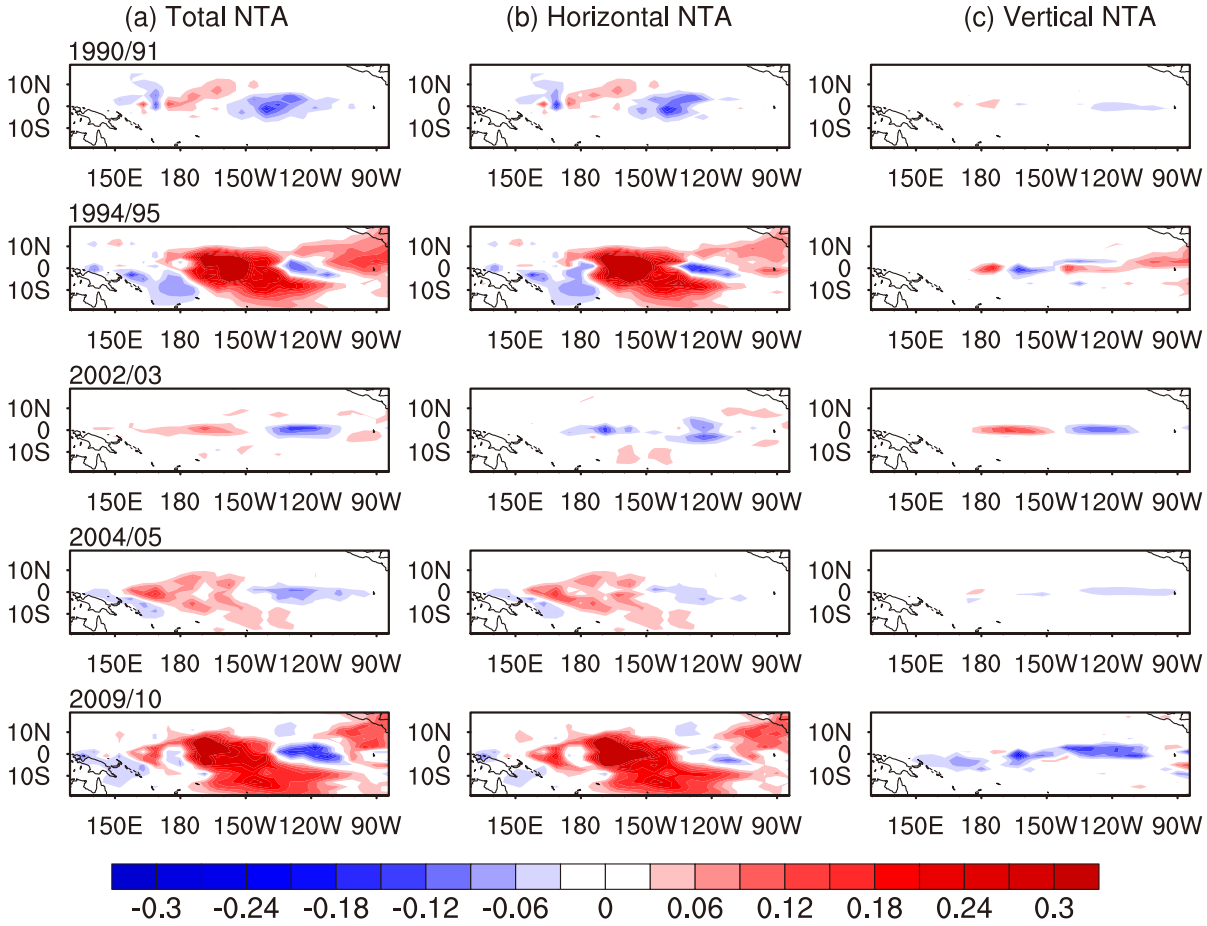

Fig. 7. Spatial structures of (a) the NTA [units: °C (10 d)$^{-1}$] and (b) its horizontal and (c) vertical components in the mature phases of five CP El Niño events. NTAs are plotted for January 1991, January 1995, November 2002, January 2005, and January 2010.

dition enhances the anomalous easterly wind and hinders the movement of warm water in the central Pacific towards the east. Differences in the relative intensity of these scenarios determine that the shifting of the warm center of CP El Niño events occurs in the central Pacific. Figure 8 demonstrates that the zonal wind in the nonlinear Zebiak–Cane model is a westerly wind anomaly in the Niño4 region and an easterly wind anomaly in the Niño3 region, but that the linearized model presents an easterly wind anomaly in the Niño4 region and a negligible wind anomaly in the Niño3 region. These differences between the nonlinear and linearized models reflect the effects of NTA feedback, which demonstrate that the anomalous westerly wind induced by the NTA over the central-western Pacific is a little larger than, or almost equal to, the anomalous easterly wind over the central-eastern Pacific (Fig. 8c). This causes the warm center of a CP El Niño event to move slightly eastwards, or to keep its location unchanged. Clearly, the shift of the warm centers of these CP El Niño events is subject to the NTA-induced wind gradient between the anomalous westerly wind in the western Pacific and the anomalous easterly wind in the eastern Pacific. Although the 1994/95 and 2009/10 events feature much larger positive NTA values and are significantly enhanced by the NTA, they may involve slightly different NTA-induced wind gradients than those observed in the 1990/91, 2002/03, and 2004/05 events, thus suggesting that the NTA has almost the same effect on the spatial structure of strong CP El Niño events as it does on those of weak CP El Niño events. Furthermore, this effect is less significant on CP El Niño events. Therefore, these data, along with those of the linearized model also presenting CP El Niño–like events, suggest that nonlinearity plays only a minor role in selecting CP El Niño events.

3.2. *EP El Niño events*

In this section, we perform numerical experiments similar to those performed for the previously discussed CP El Niño events, for each of the four reproduced EP El Niño events shown in Fig. 2. Figure 9 plots the evolution of EP El Niño events reproduced by the nonlinear Zebiak–Cane model, as well as those of the corresponding El Niño-like events in the linearized Zebiak–Cane model. These results demonstrate that, after the Zebiak–Cane model is linearized, the warm center of EP El Niño events moves significantly westwards. As a result, the El Niño-like events in the linearized model

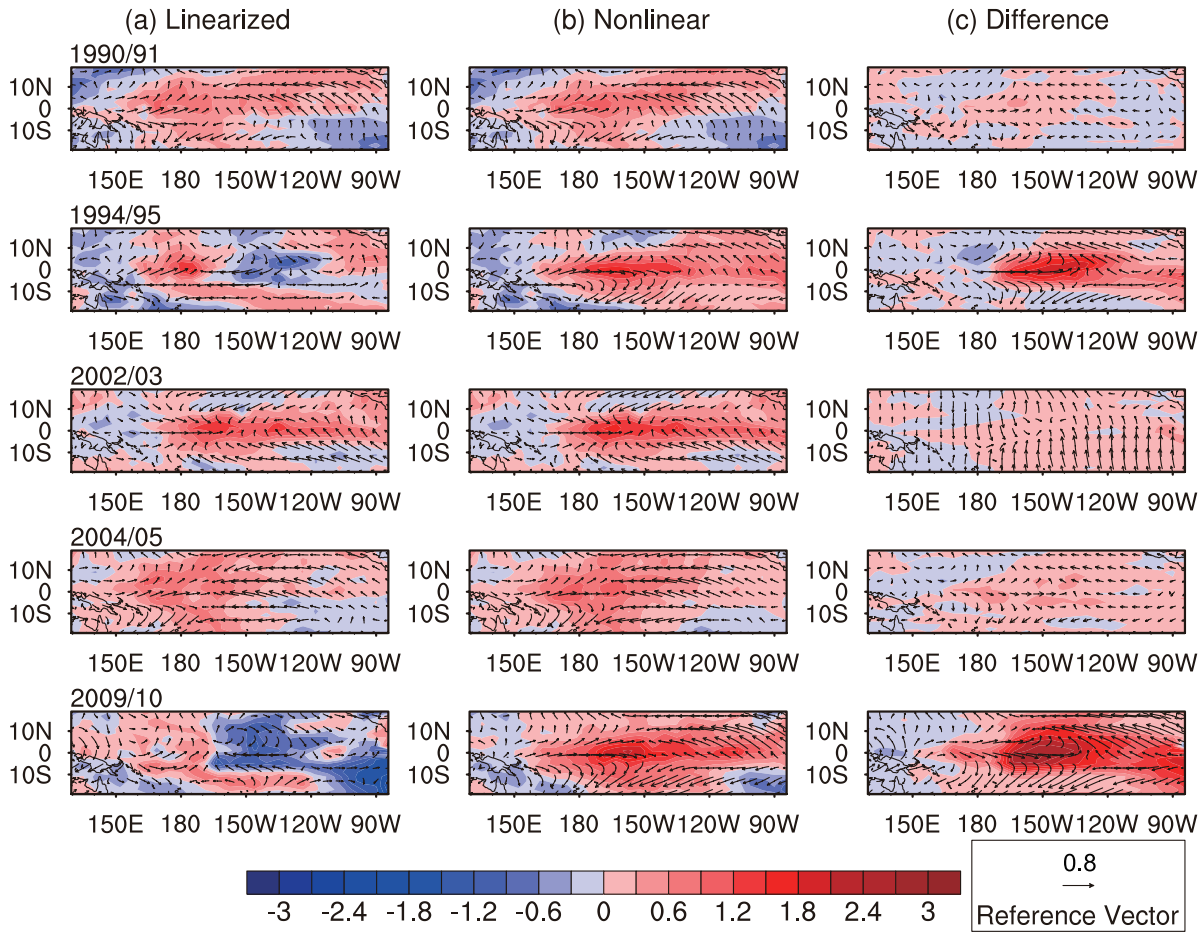

Fig. 8. Wind anomaly fields (vectors; units: m s^{-1}) and SSTA (units: °C) in the mature phases (shaded) of five CP El Niño events: (a) results of El Niño events reproduced by the linearized Zebiak–Cane model; (b) results of El Niño events generated by the nonlinear Zebiak–Cane model; (c) differences between (b) and (a). Fields are plotted for January 1991, January 1995, November 2002, January 2005, and January 2010.

corresponding to the 1986/87 event tend to be CP El Niño-like events; the 1972/73 and 1997/98 El Niño events initially present their warming centers in the eastern tropical Pacific, but they eventually move to the central tropical Pacific. These data indicate that El Niño-like events in the linearized Zebiak-Cane model tend to be CP El Niño–like events when reaching the peak of the observed ones, with the exception of the 1982/83 event. They also suggest that the nonlinearity of the Zebiak–Cane model often moves the warm center of El Niño events significantly eastwards. Meanwhile, comparing the reproduced EP El Niño events in the nonlinear model with the El Niño-like events in the linearized model indicates that nonlinearity consistently enhances the intensities of four EP El Niño events, particularly during the mature phases of these events (i.e., in January of the 1972, 1982, 1986, and 1997 El Niño years), thus supporting the previous results of An and Jin (2004) and Duan et al. (2004, 2008) on nonlinearity modulating ENSO amplitudes.

Figure 4 demonstrates that the NTA values of all EP El Niño events, except for the 1982/83 event, are significantly larger in their amplitudes than the damping difference. Especially during the mature phases of EP El Niño events, the NTA is positive when the damping term change is negative, demonstrating that the NTA most significantly enhances EP El Niño events. Figure 10 displays the time-dependent evolution of the NTA along the equator associated with EP El Niño events. This figure demonstrates that the positive NTA of all EP El Niño events, except for the 1982/83 El Niño event, tends to appear first in the eastern equatorial Pacific, and then extends westwards, before finally making the warming rate of the NTA occur throughout almost the entire tropical eastern Pacific and reach its maximum during the mature phase of the El Niño event. This explains why nonlinearity enhances EP El Niño events, especially during their mature phases. Comparing the horizontal and vertical NTAs further demonstrates that the former value tends to be considerably larger for strong EP El Niño events (i.e., the 1972/73 and 1997/98 events) than it is for weak ones (i.e., the 1986/87 event), while the latter displays less of a significant difference between strong and weak events. Additionally, the amplitude of the former value is often significantly larger than that of the latter, suggesting that the former plays a dominant role in

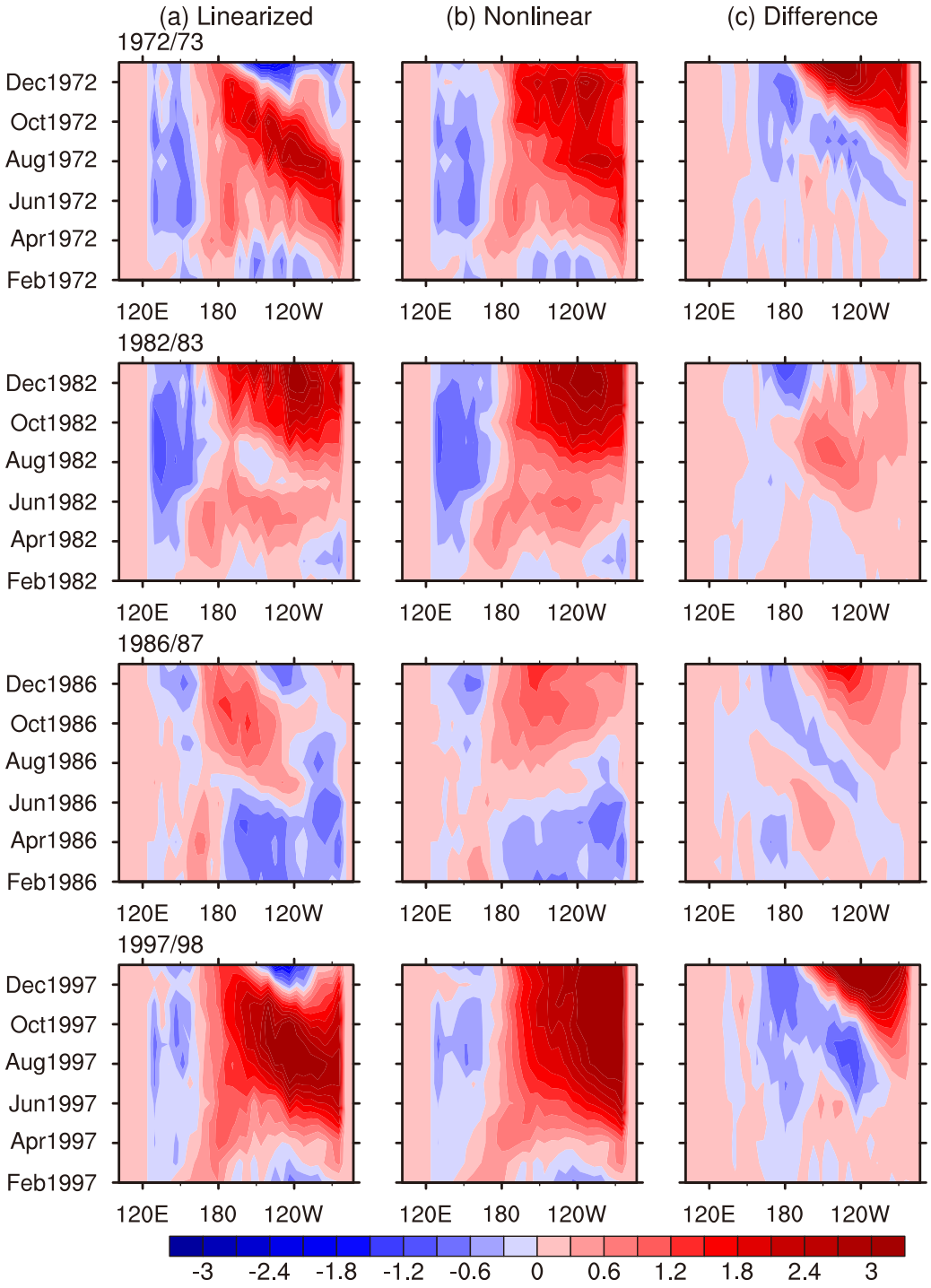

Fig. 9. As in Fig. 5 but for EP El Niño events.

enhancing EP El Niño events. Despite the fact that the vertical NTA component involves relatively small amplitudes, it does uniformly present positive values in the eastern equatorial Pacific during the mature phases of events, which can also help increase the SSTAs in the eastern equatorial Pacific, but may play a secondary role in enhancing EP El Niño events.

Figure 11 displays the NTA, and its horizontal and vertical components, during the mature phases of EP El Niño events. This figure illustrates that the NTA presents positive values in the tropical central and eastern Pacific and that its horizontal component contributes most significantly to it. The positive NTA in the Niño3 region, especially the positive horizontal NTA, then increases the positive SSTA in the same area in the nonlinear Zebiak–Cane model. These increasing SSTAs cause the zonal SST difference to increase and generate stronger westerly anomalies in the tropical central Pacific (Fig. 12). This not only causes warm water to move towards the east, but also weakens the anomalous upwelling

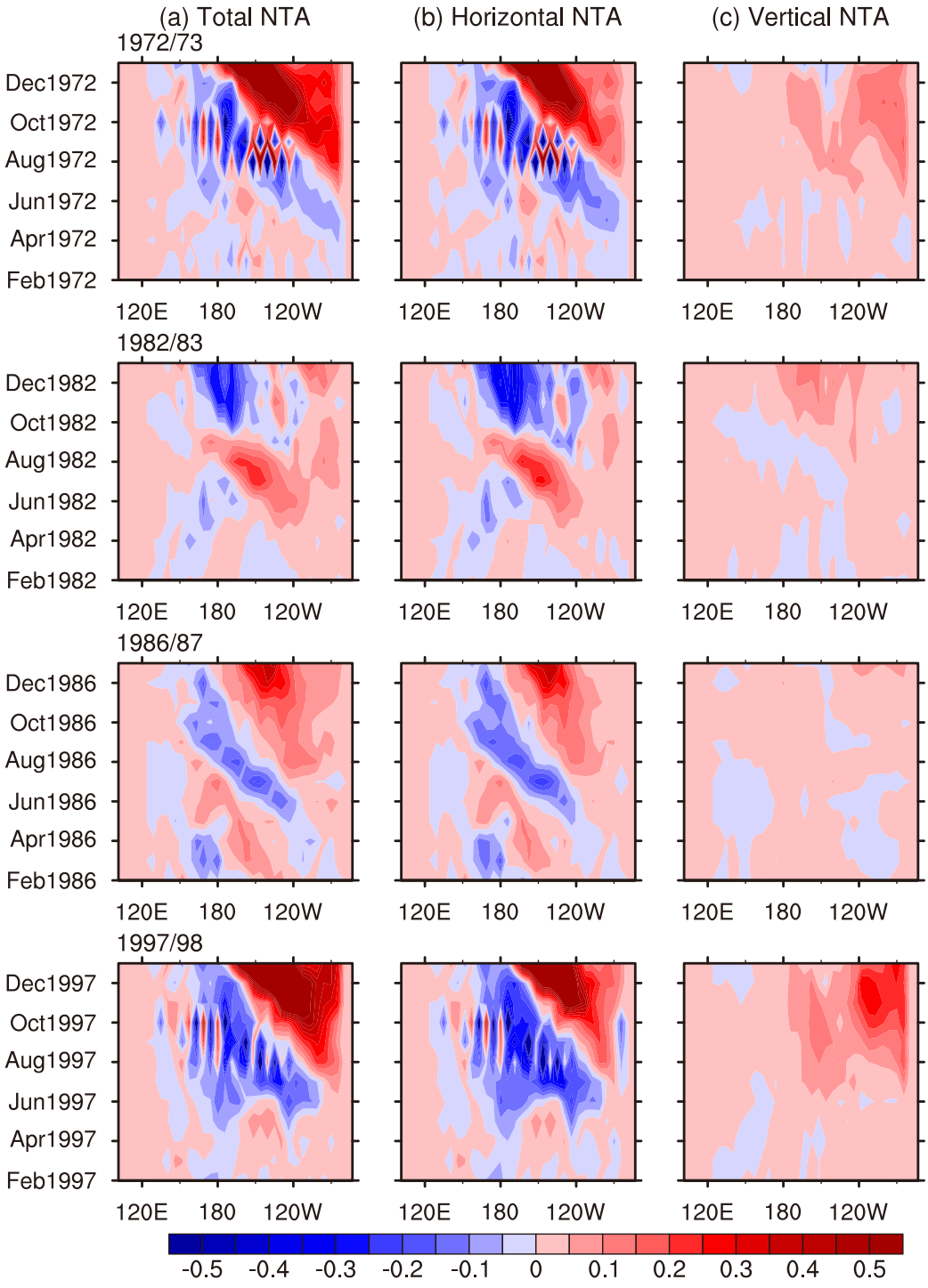

Fig. 10. As in Fig. 6 but for EP El Niño events.

of cold water in the tropical eastern Pacific, finally resulting in the strengthening of the EP El Niño event and causing the warm center of EP El Niño events to move markedly eastwards. These results demonstrate that all El Niño-like events (except for the 1982/83 event) in the linearized model are much more like CP El Niño events, but that the events affected by NTA (i.e., those in the nonlinear Zebiak–Cane model) present more eastward warm centers and tend to be EP El Niño events. Therefore, we conclude that the NTA significantly promotes EP El Niño events.

4. Contrasting CP and EP El Niño events

Thus far, we have demonstrated that the NTA associated with the mature phases of CP El Niño events is positively stronger over the central Pacific than it is over other regions

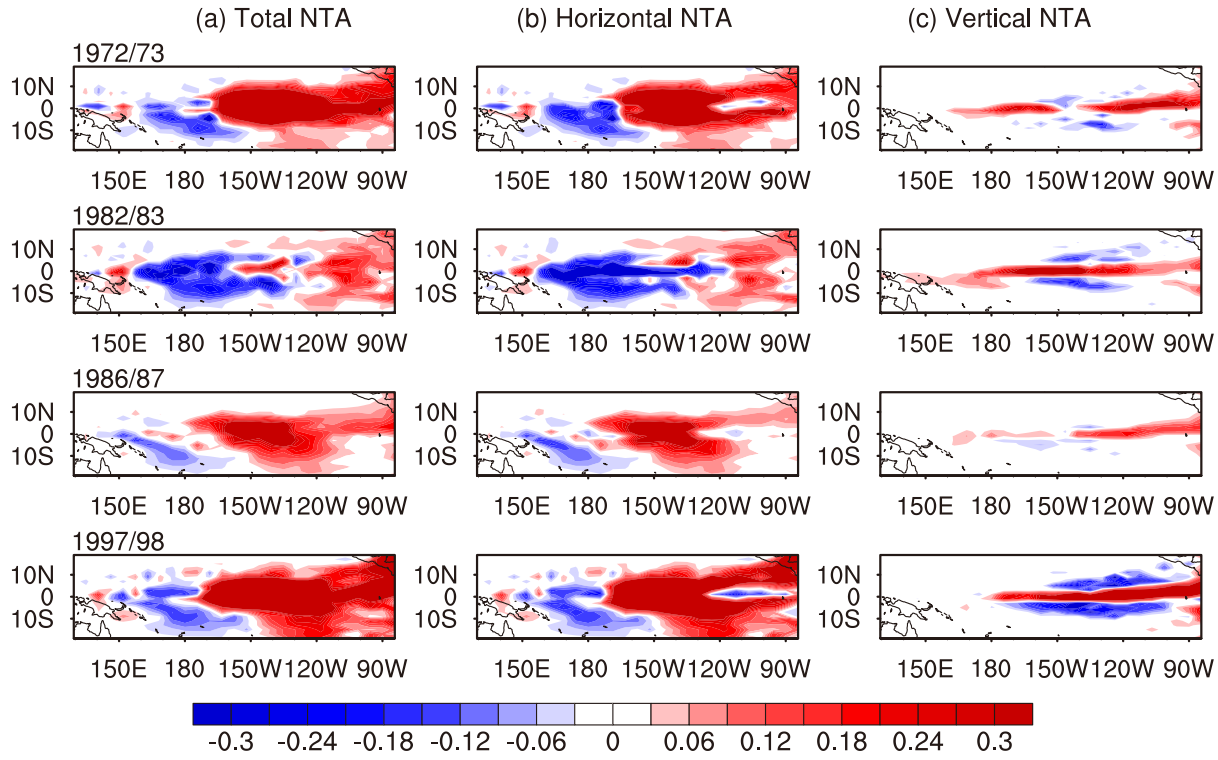

Fig. 11. Spatial structures of (a) the NTA [units: °C (10 d)$^{-1}$] and (b) its horizontal and (c) vertical components in the mature phases of four EP El Niño events. NTAs are plotted for January 1972, 1983, 1987, and 1998.

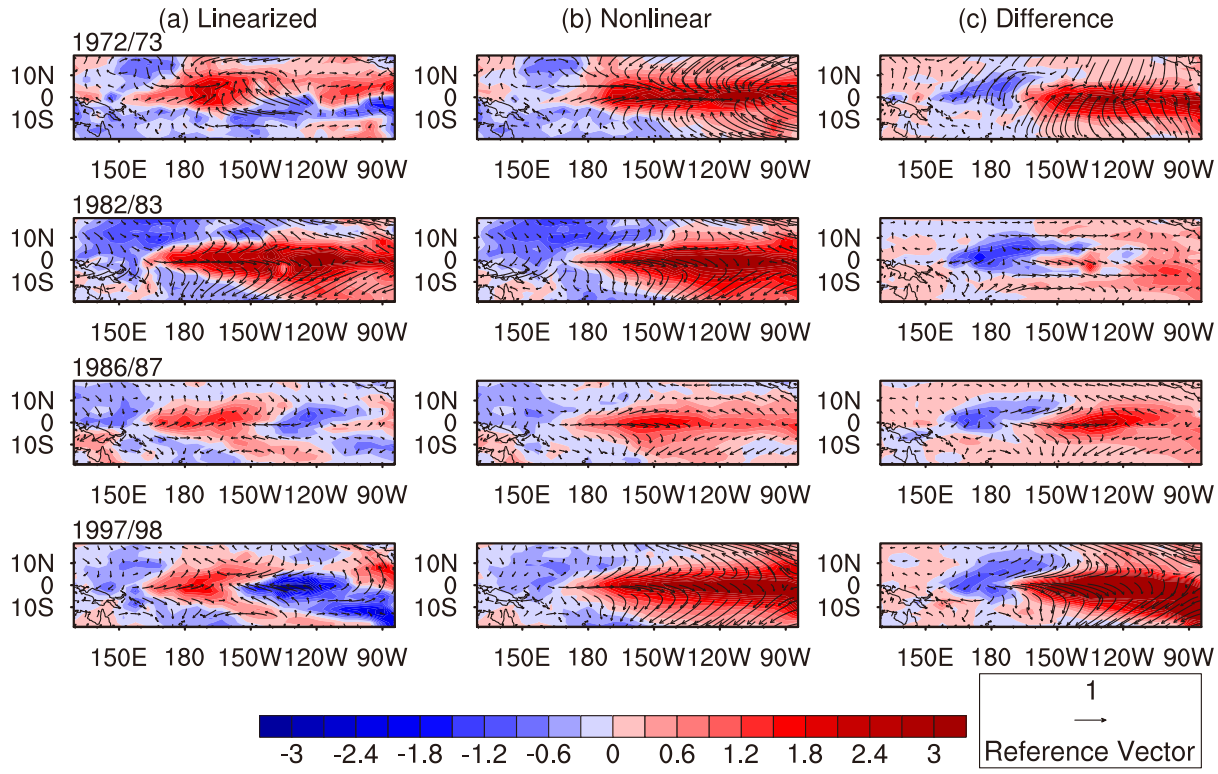

Fig. 12. Wind anomaly fields (vectors; units: m s^{-1}) and SSTA (units: °C) in the mature phases (shaded) of four EP El Niño events: (a) results of El Niño events reproduced by the linearized Zebiak–Cane model; (b) results of the El Niño events generated by the nonlinear Zebiak–Cane model; and (c) differences between (b) and (a). Fields are plotted for January 1972, 1983, 1987, and 1998.

(Fig. 7). This NTA has a negligible effect on weak CP El Niño events, as it only minimally influences their intensities, but has a considerable impact on strong CP El Niño events by significantly amplifying them. The positive NTA associated with CP El Niño events is located in the Niño4 region and induces an anomalous westerly–easterly wind contrast between the tropical western Pacific and the tropical eastern Pacific. These westerly and easterly winds almost balance each other, thus causing the location of the warm center of CP El Niño events to not change significantly from that of the linearized Zebiak–Cane model, thus implying that the NTA plays a minor role in selecting CP El Niño events. However, in EP El Niño events, the related NTA is much stronger over the eastern Pacific than it is over other regions (Fig. 11); this NTA is thus inclined to significantly enhance the intensities of EP El Niño events. However, this NTA favors the warm center of CP El Niño–like events presented in the linearized Zebiak–Cane model to be situated far more eastwards, and tends to yield EP El Niño events in the nonlinear Zebiak–Cane model. Regardless, whether using EP or CP El Niño event reference states, the relevant linearized Zebiak–Cane models tends to yield CP El Niño–like events. However, the NTA of CP El Niño events tends to not alter the structure of CP El Niño–like events shown in the linearized Zebiak–Cane model, whereas the NTA of EP El Niño events pushes the warm center of CP El Niño-like events markedly eastwards, finally producing EP El Niño events in the nonlinear Zebiak–Cane model. Therefore, we conclude that, in making a distinction between El Niño types, nonlinearity considerably promotes EP El Niño events. The amplitude of the NTA is much smaller in the Niño4 region for CP El Niño events than it is in the Niño3 region for EP El Niño events (Fig. 13), thus explaining why EP El Niño events are often stronger than CP El Niño events.

5. Summary and discussion

In this study, we use an OFV approach to reproduce five CP El Niño events and four EP El Niño events to reveal the comparative influence of the nonlinear temperature advection on the intensities and spatial modes of CP and EP El Niño events. The results demonstrate the influence of nonlinear temperature advection is mainly from the NTA (i.e., nonlinearly induced temperature advection change). The NTA yields different amplitudes and spatial distributions for CP and EP El Niño events, and thus has different influences on the intensities and spatial structures of the two types of El Niño events. For CP El Niño events, the NTA presents positive anomalies in the tropical central Pacific and shows a center-strong and east- and west-weak (sometimes east- and west-negative) structure along the equatorial Pacific. These structures increase the central Pacific (especially in the Niño4 region) positive SSTA of CP El Niño (especially for strong CP El Niño events), which induces a westerly wind anomaly over the tropical central-western Pacific and an easterly wind anomaly over the tropical central-eastern Pacific. These anomalies almost balance each other and eventually cause the warm center of CP El Niño events to remain essentially unmoved. For EP El Niño events, the NTA presents positive

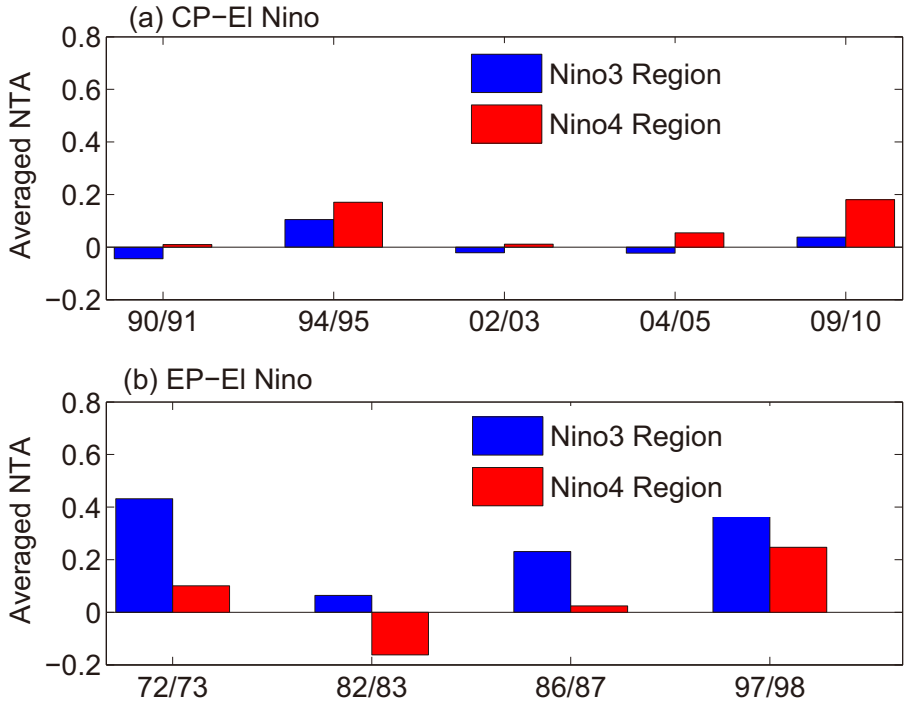

Fig. 13. Values of NTA [units: °C (10 d)$^{-1}$] averaged over the Niño3 and Niño4 regions in the mature phases of (a) five CP El Niño events plotted for January 1991, January 1995, November 2002, January 2005, and January 2010; and (b) four EP El Niño events plotted for January 1972, 1983, 1987, and 1998.

anomalies in the tropical eastern Pacific, and an east-strong and west-weak (sometimes negative) structure. This effect then enhances the tropical eastern Pacific positive SSTA of EP El Niño events, generating westerly anomalies in the tropical central Pacific and finally favoring warm water in the east and a weakening of the anomalous upwelling of cold water in the tropical eastern Pacific. These combined effects result in the NTA enhancing the strength of EP El Niño events and moving the warm center to the east, ultimately causing the CP El Niño–like events in the linearized Zebiak–Cane model to become EP El Niño events in the nonlinear Zebiak–Cane model.

The NTA of CP El Niño events is smaller in its amplitude than that of EP El Niño events. Correspondingly, the amplitude of CP El Niño events is weakly influenced by nonlinearities, whereas the amplitude of EP El Niño events is significantly enhanced, thus explaining why EP El Niño events are often stronger than CP El Niño events. Additionally, based on the fact that nonlinearities do not significantly affect the spatial mode of CP El Niño events, but do significantly promote EP El Niño events, we can deduce that CP El Niño events may be controlled by a weak nonlinearity and that EP El Niño events may be modulated by a relatively strong nonlinearity. Considering that the NTA values of CP and EP El Niño events possess different spatial characteristics and intensities, therefore producing relatively weak CP and relatively strong EP El Niño structures, the suggestion is that the diversity of El Niño events may be closely related to changes in nonlinear characteristics within the tropical Pacific.

As previously mentioned, the reasons for the frequent occurrence of CP El Niño events in recent decades remain controversial. In the present study, we argue that changes in the nonlinearity of ENSO are responsible for El Niño diversity. This conclusion is different from explanations proposed by previous researchers, such as a La Niña-like tropical Pacific, global warming, and westerly wind bursts (see introduction for more details), and may represent a new viewpoint for better understanding the causes of ENSO diversity. However, the results obtained in the present study are based on an intermediate complex model (more specifically, a forcefully corrected intermediate complex model). The resulting conclusions are therefore indicative, and should be further confirmed by future work that examines the results of changes in OFVs or uses a much more complete and realistic climate model that can reproduce the two types of El Niño events.

In the present study, we emphasize that the spatial structure of CP El Niño events is trivially influenced by the NTA and that the linearized Zebiak–Cane model also produces CP El Niño-like events. These results indicate that CP El Niño events are mainly controlled by a linear system. In fact, the linear framework of the Zebiak–Cane model is mainly influenced by the linear temperature advection process. Therefore, we infer that the linear temperature advection process plays an important role in the development of CP El Niño events, which supports the viewpoint of Su et al. (2014). Some studies have demonstrated that linear temperature advections are also dominant in EP El Niño events (e.g., Guan and McPhaden, 2016). Herein, we demonstrate that the linearized Zebiak–Cane model can still produce CP El Niño-like events, with the exception of the 1982/83 EP El Niño event; however, when the NTA is superimposed on the model, these events become EP El Niño events. These results stress the importance of the NTA in the distinction of EP El Niño events. Future work is needed to determine whether linear temperature advection or the NTA play a more important role in the distinction of EP El Niño structures.

The present study corrects the Zebiak–Cane model to demonstrate that CP El Niño events tend to be controlled by weak nonlinearity, whereas EP El Niño events are likely to be modulated by strong nonlinearity. Strong nonlinearity is much more likely to cause irregularities in ENSO and limit its predictability. Therefore, these results indicate that it may be easier to predict CP El Niño events than EP El Niño events, if the effects of model error can be neglected. In fact, Tian and Duan (2016) demonstrated that CP El Niño events are less influenced by the spring predictability barrier for ENSO forecasting, implying that they are more predictable than EP El Niño events. Hendon et al. (2009) further indicated that the predictive skill of the Niño4 index features much less of a spring predictability barrier, and thus that it is easier to predict CP El Niño events. Despite these results, it remains highly challenging to predict which type of El Niño event will occur; future studies should therefore attempt to improve the predictability of these two types of El Niño events.

Acknowledgements. The authors thank the editor and two anonymous reviewers very much for their very insightful comments and suggestions. This work was sponsored by the National Natural Science Foundation of China (Grant Nos. 41525017, 41230420 and 41476015).

APPENDIX A

Nonlinear Effects of Nonlinear Temperature Advection in the Zebiak–Cane Model

The SSTA equation in the (corrected) Zebiak–Cane model can be written as

$$\frac{\partial T}{\partial t} = \Psi_{\rm h} + \Psi_{\rm v} - \alpha_s T + f \,, \tag{A1}$$

where "f" is the OFV (Duan et al., 2014) superimposed on the SSTA equation and is used to correct the model. The temperature advection is

$$\begin{cases} \Psi = \Psi_{\rm h} + \Psi_{\rm v} \,, \\ \Psi_{\rm h} = -\bar{u}T_x - \bar{v}T_y - u\overline{T}_x - v\overline{T}_y - uT_x - vT_y \,, \\ \Psi_{\rm v} = -\gamma M(\bar{w})T_z - \gamma[M(\bar{w}+w) - M(\bar{w})]\overline{T}_z \\ \qquad\quad -\gamma[M(\bar{w}+w) - M(\bar{w})]T_z \,. \end{cases} \tag{A2}$$

Here, T, u, v and w denote respectively anomalies of mixed layer temperature (or SST), horizontal surface zonal velocity, meridional velocity, and upwelling at the mixed layer base. γ is a parameter that describes the strength of upwelling with the value 0.75, and α_s is a nondimensional parameter

that represents the Newtonian cooling coefficient for SSTA. $M(x)$ is defined by $M(x) = \begin{cases} 0, & x \leqslant 0; \\ x, & x > 0. \end{cases}$ The overbar denotes the climatological mean; and $\Psi_{\rm h}$ and $\Psi_{\rm v}$ represent the horizontal and vertical components, respectively, of the temperature advection Ψ. The term $\Psi_{\rm n} = -uT_x - vT_y - \gamma[M(\bar{w}+w) - M(\bar{w})]T_z$, which comprises the same nonlinear terms as $\Psi_{\rm h}$ and $\Psi_{\rm v}$, is called nonlinear temperature advection and represents the nonlinear term of the Zebiak–Cane model.

To reveal the effects of nonlinear temperature advection, we linearize Eq. (A1) as follows:

$$\frac{\partial T'}{\partial t} = \Psi'_{\rm h} + \Psi'_{\rm v} - \alpha_s T' + f \,, \tag{A3}$$

where "f" is the same as in Eq. (A1), and the prime denotes the variables in the linearized model. The temperature advections in the linearized model then become

$$\begin{cases} \Psi' = \Psi'_{\rm h} + \Psi'_{\rm v} \,, \\ \Psi'_{\rm h} = -\bar{u}T'_x - \bar{v}T'_y - u'\overline{T}_x - v'\overline{T}_y \,, \\ \Psi'_{\rm v} = -\gamma M(\bar{w})T'_z - \gamma[M(\bar{w}+w') - M(\bar{w})]\overline{T}_z \,, \end{cases} \tag{A4}$$

where $\Psi'_{\rm h}$ and $\Psi'_{\rm v}$ are the horizontal and vertical components, respectively, of the temperature advection in the linearized model.

The differences between the nonlinear and linear model reflect the full role of nonlinear temperature advection in modulating SSTA. As such, we subtract Eq. (A3) from Eq. (A1) to obtain the difference between the SSTA in the nonlinear model and that in the linearized model:

$$\frac{\partial (T - T')}{\partial t} = (\Psi_{\rm h} - \Psi'_{\rm h}) + (\Psi_{\rm v} - \Psi'_{\rm v}) - \alpha_s (T - T') \,, \tag{A5}$$

where

$$\begin{aligned} \Psi_{\rm h} - \Psi'_{\rm h} &= -\bar{u}T_x - \bar{v}T_y - u\overline{T}_x - v\overline{T}_y - uT_x - vT_y \\ &\quad -(-\bar{u}T'_x - \bar{v}T'_y - u'\overline{T}_x - v'\overline{T}_y) \\ &= -\bar{u}(T - T')_x - \bar{v}(T - T')_y - (u - u')\overline{T}_x \\ &\quad -(v - v')\overline{T}_y - uT_x - vT_y \,, \\ \Psi_{\rm v} - \Psi'_{\rm v} &= -\gamma M(\bar{w})T_z - \gamma[M(\bar{w}+w) - M(\bar{w})]\overline{T}_z \\ &\quad -\gamma[M(\bar{w}+w) - M(\bar{w})]T_z \\ &\quad -\{-\gamma M(\bar{w})T'_z - \gamma[M(\bar{w}+w') - M(\bar{w})]\overline{T}_z\} \\ &= -\gamma M(\bar{w})(T - T')_z - \gamma[M(\bar{w}+w) - M(\bar{w}+w')]\overline{T}_z \\ &\quad -\gamma[M(\bar{w}+w) - M(\bar{w})]T_z \,. \end{aligned} \tag{A6}$$

The tendency of Eq. (A5) reveals the full effect of nonlinear temperature advection in modulating the SSTA. This nonlinearity includes not only the nonlinear terms $-uT_x - vT_y - \gamma[M(\bar{w}+w) - M(\bar{w})]T_z$ of the nonlinearly induced temperature advection change $(\Psi - \Psi')$ but also its linear terms $-\bar{u}(T - T')_x - \bar{v}(T - T')_y - (u - u')\overline{T}_x - (v - v')\overline{T}_y$ and $-\gamma M(\bar{w})(T - T')_z - \gamma[M(\bar{w}+w) - M(\bar{w}+w')]\overline{T}_z$, and the linear damping term $-\alpha_s(T - T')$. In these terms, the nonlinearly induced SSTA changes are measured by not only the nonlinearly induced temperature advection change $\Psi - \Psi' = (\Psi_{\rm h} - \Psi'_{\rm h}) + (\Psi_{\rm v} - \Psi'_{\rm v})$, but also by the damping term change $-\alpha_s(T - T')$. Equation (A5) demonstrates that the influence of nonlinear temperature advection is driven by the NTA change, where NTA is equal to $\Psi - \Psi'$, and $\Psi_{\rm h} - \Psi'_{\rm h}$ and $\Psi_{\rm v} - \Psi'_{\rm v}$ represent the horizontal and vertical components of the NTA, respectively.

APPENDIX B

The OFV Approach

Consider the following nonlinear partial differential equation:

$$\begin{cases} \dfrac{\partial \boldsymbol{u}}{\partial t} = F(\boldsymbol{u}, t) \,, \\ \boldsymbol{u}|_{t=0} = \boldsymbol{u}_0 \,, \end{cases} \tag{B1}$$

where $\boldsymbol{u}(\boldsymbol{x}, t) = [u_1(\boldsymbol{x}, t), u_2(\boldsymbol{x}, t), \ldots, u_n(\boldsymbol{x}, t)]$ is the state vector, F is a nonlinear operator, $\boldsymbol{u}_0$ is the initial state, $(\boldsymbol{x}, t) \in \boldsymbol{\Omega} \times [0, T]$, $\boldsymbol{\Omega}$ is a domain in $\mathbf{R}^n$, $T < +\infty$, $\boldsymbol{x} = (x_1, x_2, \ldots, x_n)$, and t is time. For the given initial field $\boldsymbol{u}_0$, the solution to Eq. (1) for the state vector $\boldsymbol{u}$ at time τ is given by

$$\boldsymbol{u}(\boldsymbol{x}, \tau) = \boldsymbol{M}_\tau(\boldsymbol{u}_0) \,. \tag{B2}$$

The model described by Eq. (B1) can be used to predict the motion of the atmosphere or ocean. However, errors are associated with this model and therefore yield prediction uncertainties. To superimpose a time-variant external forcing to offset the effects of these model errors, one must obtain a proper external forcing $\boldsymbol{f}(\boldsymbol{x}, t)$ for Eq. (B3) to force the model to agree with observations:

$$\begin{cases} \dfrac{\partial \boldsymbol{u}}{\partial t} = F(\boldsymbol{u}, t) + \boldsymbol{f}(\boldsymbol{x}, t) \,, \\ \boldsymbol{u}|_{t=0} = \boldsymbol{u}_0 \,. \end{cases} \tag{B3}$$

Therefore, this problem can be expressed as a nonlinear optimization problem. The optimization problem can consider that certain $\boldsymbol{f}(\boldsymbol{x}, t)$ are chosen to minimize the differences between the model simulation and the observations. An external forcing should be chosen to satisfy the following optimization problem:

$$J(\boldsymbol{f}_{\min,t_i}) = \min \| \boldsymbol{M}_{t_{i+1}-t_i}(\boldsymbol{f}_{t_i})(\boldsymbol{u}_{t_i}) - \boldsymbol{u}_{{\rm obs},t_{i+1}} \| \,, \tag{B4}$$

where $t_i, t_{i+1} \in [t_0, t_k]$, $\boldsymbol{M}_{t_{i+1}-t_i}(\boldsymbol{f}_{t_i})$ is the propagator of Eq. (B3) from time t_i to t_{i+1}, and $\boldsymbol{u} = \boldsymbol{M}_{t_i - t_{i-1}}(\boldsymbol{f}_{\min,t_{i-1}})(\boldsymbol{u}_{t_{i-1}})$. Note that the time interval $[t_i, t_{i+1}]$ is not necessarily a time step of numerical integration, but may represent several days, a month, or a season, among others. An external forcing (vector) $\boldsymbol{f}_{\min,t_k - t_0} = (f_{\min,t_0}, f_{\min,t_1}, f_{\min,t_2}, \ldots, f_{\min,t_{k-1}})$ can be obtained from Eq. (B4). This forcing vector $\boldsymbol{f}_{\min,t_k - t_0}$ represents the OFV, which produces model simulations closest to observations during the time window $[t_0, t_k]$.

For a given norm, Eq. (B4) defines an unconstrained optimization problem, with the OFV $\boldsymbol{f}_{\min,t_k - t_0}$ representing the minimum point of the objective function in the phase space. We note that the OFV is still time-independent during the time interval $[t_i, t_{i+1}]$. Therefore, the OFV can be computed

as a constant FSV, as proposed by Barkmeijer et al. (2003), by using the limited memory Broyden–Fletcher–Goldfarb–Shanno (L-BFGS; Liu and Nocedal, 1989) algorithm. This algorithm adopts the gradient-steepest descent method and finds the minimum value of an objective function, in which one needs to calculate the gradient of the objective function with respect to the external forcing. The approach of Feng and Duan (2013) is used to numerically compute the gradient of the objective function with respect to the external forcing [see Feng and Duan (2013) for more details of this approach]. Using this gradient information, we can compute the OFV of a numerical model using the L-BFGS solver.

REFERENCES

An, S.-I., and F. F. Jin, 2004: Nonlinearity and asymmetry of ENSO. *J. Climate*, **17**, 2399–2412.

Ashok, K., S. K. Behera, S. A. Rao, H. Y. Weng, and T. Yamagata, 2007: El Niño Modoki and its possible teleconnection. *J. Geophys. Res.*, **112**, doi: 10.1029/2006JC003798.

Barkmeijer, J., T. Iversen, and T. N. Palmer, 2003: Forcing singular vectors and other sensitive model structures. *Quart. J. Roy. Meteor. Soc.*, **129**, 2401–2423.

Battisti, D. S., 1988: Dynamics and thermodynamics of a warming event in a coupled tropical atmosphere-ocean model. *J. Atmos. Sci.*, **45**, 2889–2919.

Bellenger, H., E. Guilyardi, J. Leloup, M. Lengaigne, and J. Vialard, 2014: ENSO representation in climate models: From CMIP3 to CMIP5. *Climate Dyn.*, **42**, 1999–2018, doi: 10.1007/s000382-013-1783-z.

Bjerknes, J., 1969: Atmospheric teleconnections from the equatorial Pacific. *Mon. Wea. Rev.*, **97**, 163–172.

Chen, D. K., S. E. Zebiak, A. J. Busalacchi, and M. A. Cane, 1995: An improved procedure for EI Niño forecasting: Implications for predictability. *Science*, **269**, 1699–1702.

Chen, D. K., M. A. Cane, A. Kaplan, S. E. Zebiak, and D. J. Huang, 2004: Predictability of El Niño over the past 148 years. *Nature*, **428**, 733–736.

Chen, D. K., and Coauthors, 2015: Strong influence of westerly wind bursts on El Niño diversity. *Nature Geoscience*, **8**, 339–345, doi: 10.1038/ngeo2399.

Chung, P.-H., and T. Li, 2013: Interdecadal relationship between the mean state and El Niño types. *J. Climate*, **26**, 361–379.

Duan, W. S., and M. Mu, 2006: Investigating decadal variability of El Niño–Southern Oscillation asymmetry by conditional nonlinear optimal perturbation. *J. Geophys. Res.*, **111**, doi: 10.1029/2005JC003458.

Duan, W. S., M. Mu, and B. Wang, 2004: Conditional nonlinear optimal perturbations as the optimal precursors for El Niño-Southern Oscillation events. *J. Geophys. Res.*, **109**, doi: 10.1029/2004JD004756.

Duan, W. S., H. Xu, and M. Mu, 2008: Decisive role of nonlinear temperature advection in El Niño and La Niña amplitude asymmetry. *J. Geophys. Res.*, **113**, doi: 10.1029/2006JC003974.

Duan, W. S., B. Tian, and H. Xu, 2014: Simulations of two types of El Niño events by an optimal forcing vector approach. *Climate Dyn.*, **43**, 1677–1692.

Feng, F., and W. S. Duan, 2013: The role of constant optimal forcing in correcting forecast models. *Science China Earth Sciences*, **56**, 434–443.

Feng, J., and J. P. Li, 2011: Influence of El Niño Modoki on spring rainfall over South China. *J. Geophys. Res.*, **116**, doi: 10.1029/2010JD015160.

Guan, C., and M. J. McPhaden, 2016: Ocean processes affecting the twenty-first-century shift in ENSO SST variability. *J. Climate*, **29**, doi: 10.1175/JCLI-D-15-0870.1.

Hendon, H. H., E. Lim, G. M. Wang, O. Alves, and D. Hudson, 2009: Prospects for predicting two flavors of El Niño. *Geophys. Res. Lett.*, **36**, L19713, doi: 10.1029/2009GL040100.

Jin, F.-F., 1997a: An equatorial ocean recharge paradigm for ENSO. Part I: Conceptual model. *J. Atmos. Sci.*, **54**, 811–829.

Jin, F.-F., 1997b: An equatorial ocean recharge paradigm for ENSO. Part II: A stripped-down coupled model. *J. Atmos. Sci.*, **54**, 830–847.

Kao, H.-Y., and J.-Y. Yu, 2009: Contrasting eastern-Pacific and central-Pacific types of ENSO. *J. Climate*, **22**, 615–632.

Kim, H.-M., P. J. Webster, and J. A. Curry, 2009: Impact of shifting patterns of Pacific Ocean warming on north Atlantic tropical cyclones. *Science*, **325**, 77–80.

Kim, S. T., J.-Y. Yu, A. Kumar, and H. Wang, 2012: Examination of the two types of ENSO in the NCEP CFS model and its extratropical associations. *Mon. Wea. Rev.*, **140**, 1908–1923.

Kug, J.-S., F.-F. Jin, and S.-I. An, 2009: Two types of El Niño events: Cold tongue El Niño and warm pool El Niño. *J. Climate*, **22**, 1499–1515.

Kug, J.-S., Y.-G. Ham, J.-Y. Lee, and F.-F. Jin, 2012: Corrigendum: Improved simulation of two types of El Niño in CMIP5 models. *Environ. Res. Lett.*, **7**, 034002, doi: 10.1088/1748-9326/7/3/039502.

Larkin, N. K., and D. E. Harrison, 2005: On the definition of El Niño and associated seasonal average U.S. weather anomalies. *Geophys. Res. Let.*, **32**, L13705, doi: 10.1029/2005GL022738.

Latif, M., and Coauthors, 1998: A review of the predictability and prediction of ENSO. *J. Geophys. Res.*, **103**, 14 375–14 393.

Lee, T., and M. J. McPhaden, 2010: Increasing intensity of El Niño in the central- equatorial Pacific. *Geophys. Res. Lett.*, **37**, doi: 10.1029/2010GL044007.

Li, J. P., and Coauthors, 2013: Progress in air–land–sea interactions in Asia and their role in global and Asian climate change. *Chinese Journal of Atmospheric Sciences*, **37**(2), 518–538. (in Chinese)

Liu, D. C., and J. Nocedal, 1989: On the limited memory BFGS method for large scale optimization. *Mathematical Programming*, **45**(1), 503–528.

Lopez, H., and B. P. Kirtman, 2014: WWBs, ENSO predictability, the spring barrier and extreme events. *J. Geophys. Res.*, **119**, 10 114–10 138, doi: 10.1002/2014JD021908.

McPhaden, M. J., S. E. Zebiak, and M. H. Glantz, 2006: ENSO as an integrating concept in earth science. *Science*, **314**, 1740–1745.

Mo, K. C., 2010: Interdecadal modulation of the impact of ENSO on precipitation and temperature over the United States. *J. Climate*, **23**, 3639–3656.

Na, H., B.-G. Jang, W.-M. Choi, and K.-Y. Kim, 2011: Statistical simulations of the future 50-year statistics of cold-tongue El Niño and warm pool El Niño. *Asia-Pacific Journal of Atmospheric Sciences*, **47**, 223–233, doi: 10.1007/s13143-011-0011-1.

Rasmusson, E. M., and T. H. Carpenter, 1982: Variations in tropical sea surface temperature and surface wind fields associated

with the southern oscillation/El Niño. *Mon. Wea. Rev.*, **110**, 354–384.

Rasmusson, E. M., and J. M. Wallace, 1983: Meteorological aspects of the El Niño/southern oscillation. *Science*, **222**, 1195–1202.

Rayner, N. A., D. E. Parker, E. B. Horton, C. K. Folland, L. V. Alexander, D. P. Rowell, E. C. Kent, and A. Kaplan, 2003: Global analyses of sea surface temperature, sea ice, and night marine air temperature since the late nineteenth century. *J. Geophys. Res.*, **108**, 4407, doi: 10.1029/2002JD002670.

Rosati, A., K. Miyakoda, and R. Gudgel, 1997: The impact of ocean initial conditions on ENSO forecasting with a coupled model. *Mon. Wea. Rev.*, **125**, 754–772.

Su, J. Z., R. H. Zhang, T. Li, X. Y. Rong, J.-S. Kug, and C.-C. Hong, 2010: Causes of the El Niño and La Niña amplitude asymmetry in the equatorial eastern Pacific. *J. Climate*, **23**, 605–617.

Su, J. Z., T. Li, and R. H. Zhang, 2014: The initiation and developing mechanisms of central Pacific El Niños. *J. Climate*, **27**, 4473–4485.

Takahashi, K., A. Montecinos, K. Goubanova, and B. Dewitte, 2011: ENSO regimes: Reinterpreting the canonical and Modoki El Niño. *Geophys. Res. Lett.*, **38**, L10704, doi: 10.1029/2011GL047364.

Tang, Y. M., Z. W. Deng, X. B. Zhou, Y. J. Cheng, and D. K. Chen, 2008: Interdecadal variation of ENSO predictability in multiple models. *J. Climate*, **21**, 4811–4833.

Taschetto, A. S., A. S. Gupta, N. C. Jourdain, A. Santoso, C. C. Ummenhofer, and M. H. England, 2014: Cold tongue and warm pool ENSO events in CMIP5: Mean state and future projections. *J. Climate*, **27**, 2861–2885.

Tian, B., and W. S. Duan, 2016: Comparison of the initial errors most likely to cause a spring predictability barrier for two types of El Niño events. *Climate Dyn.*, **47**, 779–792.

Wang, C. Z., 2001: A unified oscillator model for the El Niño-Southern Oscillation. *J. Climate*, **14**, 98–115.

Wang, C. Z., and J. Picaut, 2004: Understanding ENSO physics—A review. *Earth's Climate*: *The Ocean-Atmosphere Interaction*, C. Wang, S. P. Xie and J. A. Carton, Eds., American Geophysical Union, 21–48.

Wang, C. Z., and X. Wang, 2013: Classifying El Niño Modoki I and II by different impacts on rainfall in southern china and typhoon tracks. *J. Climate*, **26**, 1322–1338.

Weisberg, R. H., and C. Z. Wang, 1997: A western Pacific oscillator paradigm for the El Niño-Southern Oscillation. *Geophys. Res. Lett.*, **24**, 779–782.

Weng, H. Y., K. Ashok, S. K. Behera, S. A. Rao, and T. Yamagata, 2007: Impacts of recent El Niño Modoki on dry/wet conditions in the Pacific rim during boreal summer. *Climate Dyn.*, **29**, 113–129.

Xiang, B. Q., B. Wang, and T. Li, 2013: A new paradigm for the predominance of standing Central Pacific Warming after the late 1990s. *Climate Dyn.*, **41**, 327–340, doi: 10.1007/s00382-012-1427-8.

Yeh, S.-W., J.-S. Kug, B. Dewitte, M.-H. Kwon, B. P. Kirtman, and F.-F. Jin, 2009: El Niño in a changing climate. *Nature*, **461**, 511–514.

Yeh, S.-W., Y.-G. Ham, and J.-Y. Lee, 2012: Changes in the tropical Pacific SST trend from CMIP3 to CMIP5 and its implication of ENSO. *J. Climate*, **25**, 7764–7771.

Yu, J.-Y., H.-Y. Kao, and T. Lee, 2010: Subtropics-related interannual sea surface temperature variability in the central equatorial Pacific. *J. Climate*, **23**, 2869–2884, doi: 10.1175/2010JCLI3171.1.

Zebiak, S. E., and M. A. Cane, 1987: A model El Niño-Southern oscillation. *Mon. Wea. Rev.*, **115**, 2262–2278.